Investigation of Hydrochemical Parameters of Water Resources in Kamarderaz Anticline Plunge in the Southwest of IRAN

Seyed Yahya Mirzaee Aranki (rogin1394@gmail.com)
Shahid Chamran University of Ahvaz
Sorour Mazrae asl
Shahid Chamran University of Ahvaz
Hosein Karimi Vardanjani
Shahid Chamran University of Ahvaz

Research Article

Keywords: Oil brine, karstic aquifer, Hydrochemical parameters, Hydrogen sulfide

Posted Date: April 5th, 2021

DOI: https://doi.org/10.21203/rs.3.rs-331133/v1

Investigation of Hydrochemical Parameters of Water Resources in Kamarderaz Anticline Plunge in the Southwest of IRAN

Seyed Yahya Mirzaee Aranki[1]*, Sorour Mazrae asl[2], Hosein Karimi Vardanjani[3]

1 Assistant professor, Department of Geology, Faculty of Earth Science, Shahid Chamran University of Ahvaz, Ahvaz, Iran. Email:

2 M.Sc. Graduated in Hydrogeology, Faculty of Earth Science, Shahid Chamran University of Ahvaz, Ahvaz, Iran.

3 Ph.D. Graduated in Hydrogeology, Faculty of Earth Science, Shahid Chamran University of Ahvaz, Ahvaz, Iran.

*** Corresponding author:** Assistant professor, Department of Geology, Faculty of Earth Science, Shahid Chamran University of Ahvaz, Ahvaz, Iran. Email: rogin1394@gmail.com

Abstract

Changes in the quality of karstic water resources affected by the proximity to sources of salinity such as evaporate formations and oil brine pose major challenges to such water resources, especially in Khuzestan province, Iran. The karstic water resources of the Kamarderaz anticline plunge in Izeh city in Khuzestan province have hampered water supply management in the region. To determine water quality and the causes of water salinity in the study area, the hydrochemical parameters of the existing water resources were accordingly evaluated. To conduct hydrochemical studies, 21 samples were collected from different water sources of Kamarderaz anticline plunge in 2017-2018. To analyze the garnered data, Piper and Durov diagrams, composite graphs, ion exchange graphs, ion correlation diagrams, salinity source diagrams and ion ratios were used. The results showed that SO_4^{2-}, Cl^-, and Ca^{2+} in the water resources of the study area were likely due to several sources including carbonate minerals, gypsum dissolution, anhydrite, halite as well as oil brine. Besides, Br/Cl, I/Cl ion ratios as well as Br-Cl and SO_4-Cl diagrams revealed the mixing of karstic freshwater with oil brine in the region. The result of TOC analysis also showed that hydrocarbon materials were present in the well of Atabaki (WT). Moreover, elemental sulfur and sulfur isotope analysis showed that the process of thermochemical sulfate reduction or bacterial sulfate reduction in the presence of hydrocarbons produced H_2S gas, and eventually penetrated the WT and WH1.

Keywords: Oil brine, karstic aquifer, Hydrochemical parameters, Hydrogen sulfide

1. Introduction

Groundwater in karstic aquifers is one of the most important freshwater resources in the world, and in some areas, the only water resources available. 25% of the world's population supplies their water needs from karstic water resources (ford and Williams 2007). However, social, industrial, and agricultural developments have nowadays led to greater abstraction from groundwater resources, especially karstic aquifer resources, posing significant challenges, including reduced quality and pollution to such water resources. Therefore, water quality assessment and investigation of the origin of contamination of such resources, especially in arid and semi-arid regions, is of great importance (Jalali 2011; Mahmoudi et al. 2017; Sarikhani et al. 2015; Sefie et al. 2018; Wurbs 2011; Zarei et al. 2013). Water quality changes can be affected by human activities or environmental and structural factors associated with water reservoirs. Oil brine infiltration into karstic water resources is one of the contaminants affecting the quality of karstic aquifers (Mirzaee et al. 2019). Various causes have been identified for the salinity of karstic aquifers, including dissolution of evaporate minerals, oil brines, deep water and seawater penetration into these reservoir (Fontes and Matray 1993; Matray et al. 1994; Richter and Kreitler 1991; Rouhi and Kalantari 2018). Depending on the tectonic conditions prevailing in the folded Zagros, the carbonate formations in the region simultaneously host oil and water resources. Such proximity to oil brine, along with the presence of evaporate formations in this part of Zagros, is one of the most important factors in reducing the quality of karstic water resources in this area (Mirzaee et al. 2019).

Investigating and quantifying the salinity-related elements in water resources is thus a necessary and relatively easy task (Dogramaci and Herczeg 2002; Zaporozec 1972) but it is difficult to determine their origin (Panno et al. 1994; Sarikhani et al. 2015). In general, the penetration of hydrocarbons and oil brine in the reservoirs, as well as the presence of evaporative formations, have increased the concentration of ions and the presence of hydrocarbons, especially aromatic hydrocarbons and heavy metals in such reservoirs. In addition to minerals such as Na^{+} and Cl^{-}, oil brine contains significant amounts of Br and I ions and other secondary ions (Fan et al. 2010).

Hydrochemical evaluations generally use Na/Cl, Br/Cl and I/Cl ion ratios as well as other major Ca^{2+}, Mg^{2+}, Na^{+}, Cl^{-}, SO_4^{2-}, HCO_3^{2-} ions to distinguish salinity and mixing of saline and fresh water (Cartwright et al. 2006; Fontes and Matray 1993; Mast 1985; Matray et al. 1994; Richter and Kreitler 1991; Whittemore and Pollock 1979). The brine from the dissolution of evaporate formations increases the molar ratio of Na^{+} and Cl^{-} ions in water

(Leonard and Ward 1962). Besides, an increase in the concentration of SO_4^{2-} and Ca^{2+} due to dissolution of gypsum and anhydrite minerals in these conditions is likely. In addition to the use of ion ratios and salinity indices, the Total Organic Carbon (TOC) index can also be used to investigate the relationship of groundwater to organic matter and hydrocarbons (Chitsazan et al. 2017; Spruill 1988; Thilagavathi et al. 2016). High levels of water-soluble carbon concentration indicates the relationship of water sources with hydrocarbon materials, coal and shale formations (Thilagavathi et al. 2016). Preliminary review of studies on similar topics shows that extensive studies have been already conducted on the interference of groundwater with other sources (e.g., Tellam. 1994; Marie & Vengosh. 2001; Adams et al. 2001; Kalantari et al. 2007; Karimi & Moore. 2008; Rezai et al., 2012; Chitsazan et al., 2012; Sarikhani et al. 2015; Zega et al. 2015; Reynauld et al 2016; Mahmoudi et al. 2017; Rouhi & Kalantari. 2017; Yang et al. 2019).

Due to the lack of access to surface water flows, Izeh city in the southwestern Iran is heavily dependent on karstic water supplies. Accordingly, to supply part of the city's and its surrounding villages' drinking water in Kamarderaz anticline plunge, five water wells were drilled. During the drilling in the Atabaki area in 2016, two wells encountered H_2S gas penetration and increased Ec during drilling, making the wells unexploitable. Considering the high capacity of the aquifer in the anticline plunge, such qualitative changes occurred in this part of the aquifer posed major challenges to supplying the city's drinking water. Given the necessity of water supply for the region, analyses of hydrochemical parameters, geochemical processes, reference ion ratios (Cartwright et al. 2006; Hounslow 1995; Jean et al. 2016; Mahmoudi et al. 2017; Sarikhani et al. 2015; Whittemore and Pollock 1979) graphs of salinity source (Richter and Kreitler 1991) and TOC (Spruill 1988) were performed to investigate the causes of quality changes and also the origin of salinity.

2. Materials and methods

2.1. Study Area

Kamarderaz anticline is located northeast of Khuzestan province (southwest of Iran) and southwest of Izeh city (Figure 1). The geographical location of the anticline lies between longitude E 49° 48'18" and E 49°54'54" and latitude N 31°40'30" and N 31°46'30". Its calcareous outcrop area from the northwestern plunge to the southwestern plunge is 15 km^2, and the altitude of the northwestern plunge where it meets the plain is 830 m .According to Barangard Meteorological Station data, the average annual rainfall is 480 mm and the

average temperature is 21°C in the region, and based on meteorological parameters and Domarten classification, the climate is semi-arid.

Geology and Hydrogeology

The Zagros orogenic belt in the southwest Iran is one of the richest folded belts in the world. About 8.6% of the oil reserves and 15% of the proven gas reservoirs are stored in this belt (Sherkati and Letouzey 2004). The abundance of very rich organic rocks as well as porous and permeable reservoir rocks with suitable rock cover provide unique conditions for the production, storage and preservation of hydrocarbon materials available in the Zagros fold belt. This, in turn, makes Zagros zone one of the most oil-rich sedimentary basins in the world (Beydoun et al. 1992; Sherkati and Letouzey 2004). Carbonate sediments in this region not only host oil reservoirs, but also water resources simultaneously, as 23% of the Zagros extrusive formation are composed of karstic carbonate rocks.

The development of seams and fissures in the Zagros carbonate formation as well as the development of secondary porosities affected by tectonic activity and climatic factors have created many karstic zones in this area of Zagros and have made these formations suitable reservoirs for water storage. The folded Zagros belt shows continuous longitudinal structures such as the mountain frontal fault which are cut and displaced in different parts by transverse structures such as the Izeh fault. There is a clear structural difference between these faults by crossing Izeh's hanging wall to the Dezful embayment, the most important of which is the change in geometry and style of the folds.

Kamarderaz anticline is an asymmetric, one-sided fold which its southwestern edge, affected by tectonic activity in the region, has been severely crushed and completely destroyed except in small sections. The anticline area is very tectonically active and the outcrop formation in this anticline is mainly of Asmari calcareous formation of Oligocene-Miocene age. The Asmari formation is, in turn, composed mainly of lime, dolomite and its lower part includes the marl and anhydrite layers. In the lower part of the Asmari formation, the Pabdeh formation, which is composed of shale, marl and lime sediments with different percentages, belongs to the Paleocene-Eocene time. The Pabdeh formation on both sides restricts the eastern and western edges of the anticline.

Gachsaran evaporate formation consists mainly of evaporate minerals such as gypsum, halite, lower miocene and lower marl in the western part of the anticline. The outcrops of the

region's formations are shown in Figure 1. The karstic forms in the middle part of the formations are abundant in this anticline. The analysis of the karstic aquifer present in the anticline indicates that the aquifer has three main outcrops in the plunge section, including two springs and Halayejan wells. Total discharge rates of these three adjacent outlets are reported to be approximately 1225 liters per second according to the latest recorded data, though it dried up in 2014.

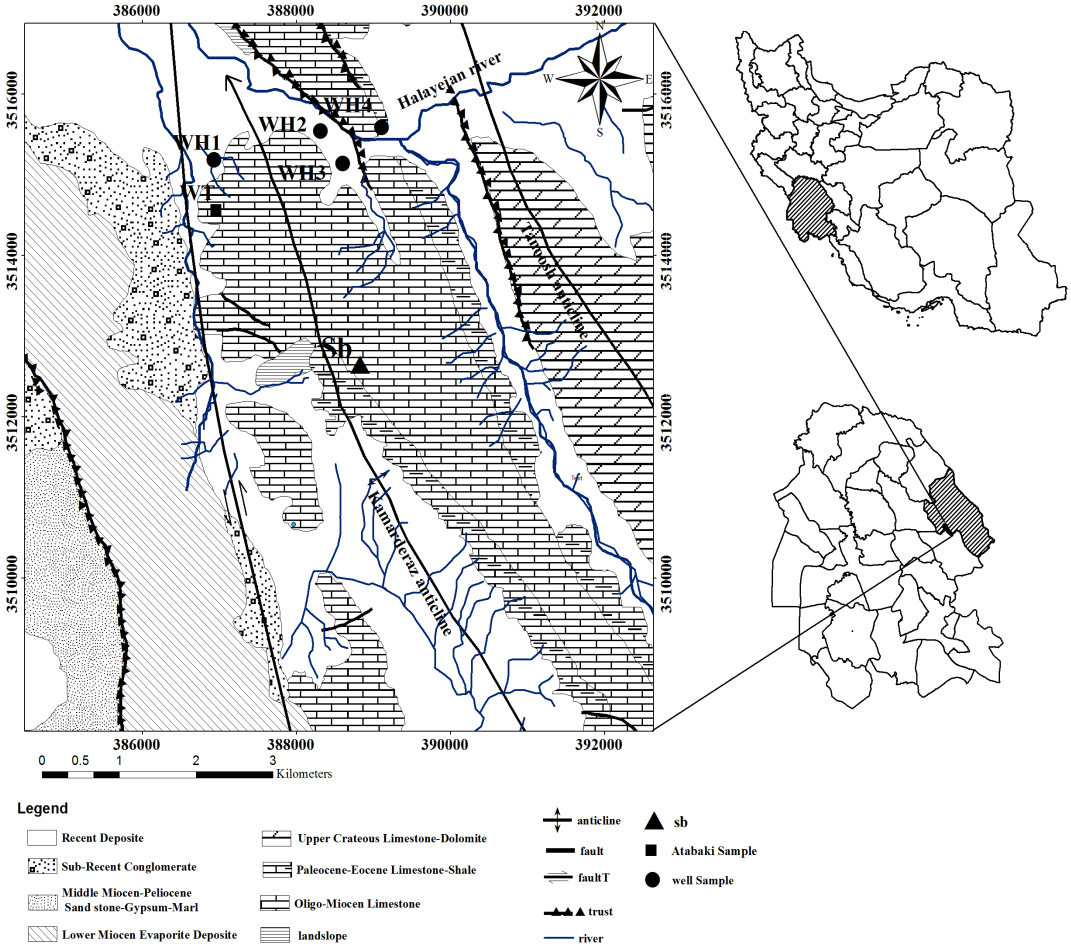

Figure 1: Location map of the study area, sampling sources and formation outcrops in the area using the 1967 Oil Company map

2.2. Sampling and Analysis

In order to perform hydrochemical studies in a wet and dry period, during four stages, 16 samples of water resources in the study area including: Halayejan wells 1, 2, 3, 4 and two samples of Bibigolmorde spring were taken. Besides, water samples collected during drilling at depths of 69, 97 and 104 m of Atabaki Well were used. The samples were collected in 1-

liter polyethylene containers and sent to the laboratories after preparation. Analysis of major anions and cations (Ca^{2+}, Na^{+}, Mg^{2+}, K^{+}, HCO_3^{2-}, SO_4^{2-}, Cl^{-}), TDS, Ec was then performed for each sample using spectrophotometer method in Khuzestan Water and Power Organization Laboratory. In turn, the analysis of Br and I ions for WHT, WH2, WH3, WH4, and WT samples was performed by red phenol colorimetric method and catalytic reduction in Aryan Fan Azma Laboratory. Total organic carbon (TOC) was measured in the Fanavar Andishe Kamyar Gostar Laboratory. Elemental sulfur in the depth of 104 m WT in was, in turn, measured in Zarazma Laboratory by spectrophotometer method. Sulfur isotopes at a depth of 104 m WT were determined by mass spectrometry at Isotpe Tech Zrt Laboratory in Hungary. The accuracy of the cation and anion analysis results was then evaluated using the following equation, which reported a data error of less than 0.5 (Equation 1).

$$\text{Ion Balance} = \frac{(\sum \text{Cat} - \sum \text{Ani})}{(\sum \text{Cat} + \sum \text{Ani})} \times 100 \quad (1)$$

Table 1 shows the results of chemical analyzes of samples taken from the sources. The anions and cations in this table are Ca^{2+}, Mg^{2+}, Na^{+}, K^{+}, Cl^{-}, HCO_3^{2-}, SO_4^{2-} in units (meq / l), (mg / l) TOC (mg / l) Br^{-}, I^{-}, (mg / l) TDS and (mmho/cm) Ec. Data obtained from hydrochemical analyzes in hydrochemical diagrams, including Piper and Durov diagrams, compound diagrams, ion exchange diagrams, ionic correlation graphs and ion ratios were used to investigate the geochemical factors, the origin of water-soluble ions, origin of salinity in the aquifer studied. The samples were then evaluated in terms of the water quality for drinking and irrigation using data from Schuler and Wilcox diagrams. Moreover, the probability of hydrocarbons in the water resources of the study area was investigated using TOC analysis.

Table 1: Hydrochemical parameters of groundwater samples

Parameters	Ca	Mg	Na	K	Hco_3	So_4	Cl	TDS	Ec	pH	Br	I
WT-69	4.52	1.72	0.91	0.05	4.4	1.78	0.82	424	642	7.8	-	-
WT-97	6.45	2.69	3.62	0.06	3.23	4.99	4.4	746	1130	7.8	-	-
WT-104	7.08	2.57	5.84	0.07	2.95	5.61	6.8	920	1438	7.9	4.91	0.018
WH1-07-17	5.13	1.84	2.51	0.05	3.73	2.72	2.88	550	860	7.3	0.93	0.033
WH1-09-17	4.37	2.43	2.51	0.04	3.22	2.87	3.06	540	844	7.5	0.62	0.012
WH1-04-18	4.67	2.1	2.99	0.04	3.67	1.73	4.2	567	914	7.5	-	-
WH1-05-18	4.53	2.28	2.6	0.04	3.71	2.5	3.04	556	868	7.5	0.74	0.019
WH2-07-17	3.17	2.13	0.58	0.02	2.94	1.88	0.88	181.2	302	7.5	-	-

WH2-09-17	3.12	2.37	0.62	0.02	3.37	1.64	0.92	287	487	7.5	-	-
WH2-04-18	3.72	0.78	0.66	0.02	3.43	0.51	1.04	285	492	7.5	-	-
WH2-05-18	3.09	1.36	0.58	0.02	3.4	0.5	0.95	289	490	7.4	0.97	0.044
WH3-07-17	3.02	1.88	0.4	0.02	3.15	1.43	0.54	246	417	7.6	-	-
WH3-09-17	3.06	1.49	0.33	0.02	2.75	1.49	0.46	267	404	7.7	-	-
WH3-04-18	3.38	0.65	0.58	0.02	3.53	0.4	0.88	257	451	6.5	-	-
WH3-05-18	3.33	1.17	0.66	0.02	3.46	0.46	1.06	321	510	7.5	0.65	0.032
WH4-07-17	4.75	1.77	0.84	0.02	3.14	2.93	1.11	346	516	7.4	-	-
WH4-09-17	2.95	1.71	1.31	0.02	2.92	1.45	1.42	358	559	7.7	-	-
WH4-04-18	3.4	1.43	1.45	0.02	3.43	1.06	1.61	333	584	7.4	-	-
WH4-05-18	3.29	1.46	1.45	0.03	3.17	1.3	1.56	385	602	7.5	0.78	0.082
Sb-07-17	2.33	1.04	0.26	0.03	2.56	0.52	0.38	158	273	7.7	-	-
Sb-09-17	1.46	1.34	0.18	0.02	2.17	0.38	0.25	149	257	7.6	-	-

3. Results and Discussion

3.1. Investigation of chemical properties of groundwater in the study area

Graphical methods are commonly used to check the quality of water resources, simplify the process of data analysis, and also determine the relationship between data gathered. The most important graphical methods for the analysis of hydrochemical data are: Piper diagram, Wilcox diagram, Schuler diagram and Stiff diagram. Piper diagrams are mainly used to identify hydrochemical facies, water type and geochemical evolution paths in aquifers. Implementation of the hydrochemical data in the Piper diagram showed that the water type in the water resources of WH2, WH3, WH4, Sb was Ca-HCO_3, while in the WH1 was Ca-Cl during September and May. Investigation of water types in WT at depths of 69, 97 and 104 m showed that the water type changed from Ca-HCO_3 to Ca-SO_4 and finally to Ca-Cl. The data scatter analysis on Piper diagram also revealed that the data from WT and WH1 were placed in the mixing zone of this graph (Fig. 2).

The Durov diagram was used to depict the characteristics of groundwater showing different hydrochemical types and processes. Samples from WH2, WH3, WH4, Sb and the 69-meter deep WT sample were located in the first square of the Durov diagram representing karstic freshwater. The WH1 and WH4 July samples as well as the 97 and 104 m WT depth samples together with September, April and May WH1 samples were located in the mixing zone of the diagram (Fig. 3). Since the formation of karstic aquifer in the region was of bicarbonate

type, bicarbonate-calcite type revealed the effect of dissolution of carbonate minerals present in such a formation on the water quality of the aquifer. However, the water type of chlorinated-calcic and sulphated-calcic in some wells and deep in the WT showed the infiltration of chlorine and sulfate from other sources into this karstic aquifer. The dissolution of evaporate minerals including gypsum and halite affected by the presence of the Gs formation (middle Oligocene Evaporate formation) as well as the mixing of aquifer with water containing high amounts of chlorine was likely the cause of these changes occurred in the region.

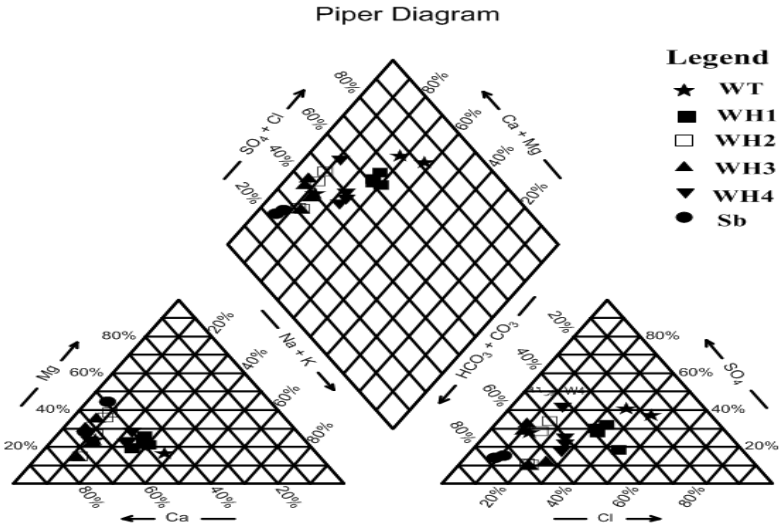

Figure 2. Representation of the studied samples in the Piper diagram

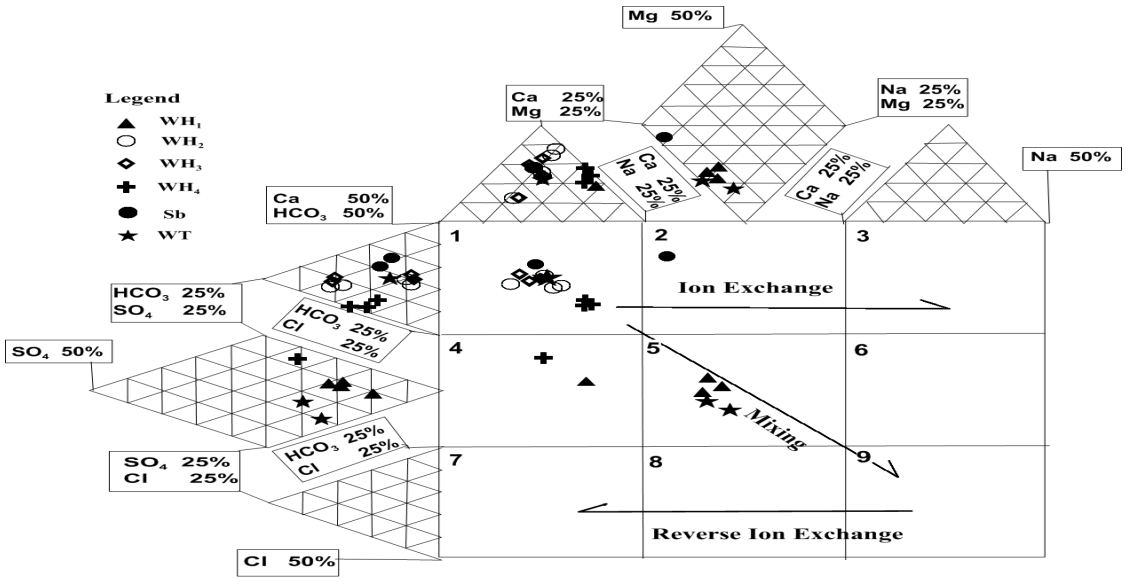

Figure 3 - Representation of samples in the expanded Durov diagram

3.2. Water quality assessment of the study area for irrigation

High concentration of some water-soluble ions, especially Na^+ in irrigation water, affects plants and soil chemically and physically. In effect, by reducing osmotic pressure, the high concentration of water-soluble ions prevents water from reaching branches and leaves, destroying the process of metabolism of plants. Sodium absorption ratio is a suitable and important parameter for agricultural water quality assessment. Salinity diagrams based on sodium absorption ratio and electrical conductivity shows water quality for irrigation, and also its alkalinity with different sodium classes. The SAR was calculated using equation 2.

$$SAR=Na^+/((Ca^{2+}+Mg^{2+})/2)^{0.5} \quad (2)$$

The calculation of sodium absorption index showed that 71.42% of samples were in C2-S1, repressinting low salinity water almost suitable for agriculture. 28.57% of the samples were in the C3-S1 range, indicating that these sources had high electrical conductivity, low SAR and generally moderate salinity risk for agriculture (Fig 4).

3.3. Water quality assessment of the study area for drinking

Given the importance of water quality for human health, it is important to assess the quality of water for drinking. Schuler diagram, as a semi-logarithmic diagram based on the major soluble ions (Ca^{2+}, Mg^{2+}, Na^+, Cl^-, HCO_3^{2-}, SO_4^{2-}) in water, is commonly used to assess the quality of watr for drinking.

Na, Cl, SO_4: All samples are suitable for drinking except WT which is within the acceptable range in terms of the concentration of this ion. TDS: All soluble solids in the WH1 and WT are within the acceptable range, and in other wells are within the appropriate range for drinking. TH: Drinking water quality in terms of total hardness parameter is acceptable for WH1, WH4, WT wells and suitable for WH2, WH3, Sb wells. Figure 5 shows the Schuler diagram for the water resources in the Kamarderaz anticline (Fig 5).

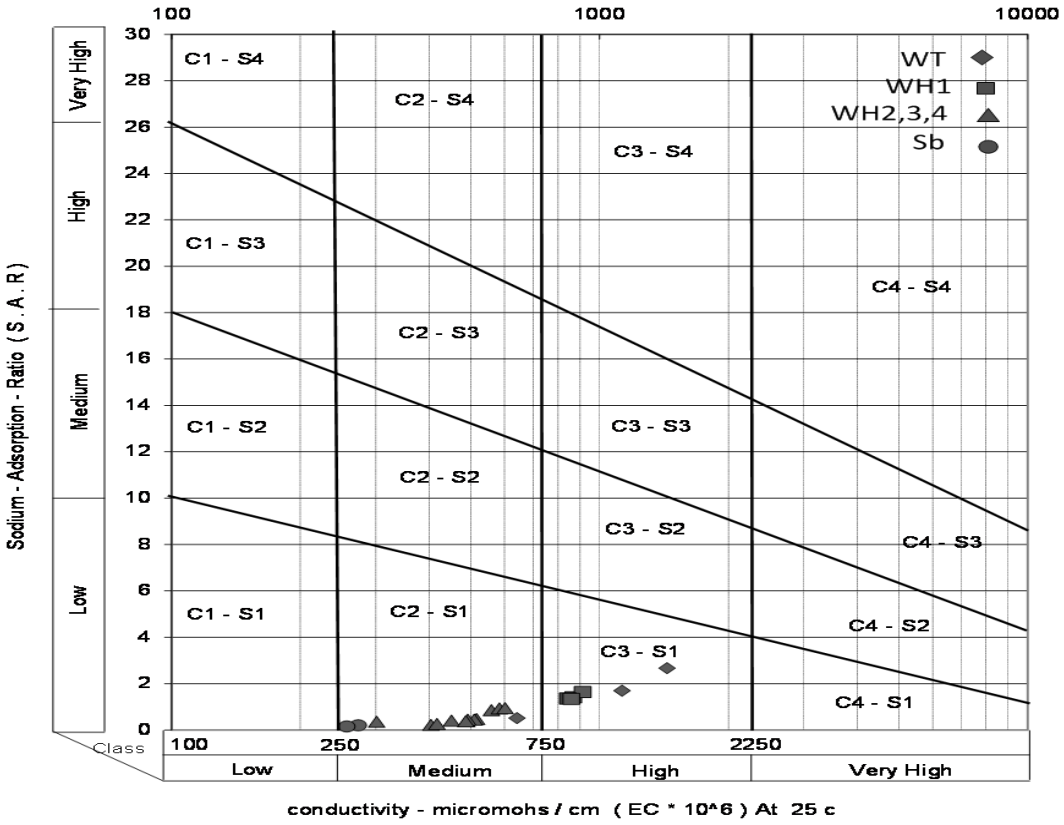

253

Figure 4. Diagram of salinity risk and alkalinity of agricultural water 254

255

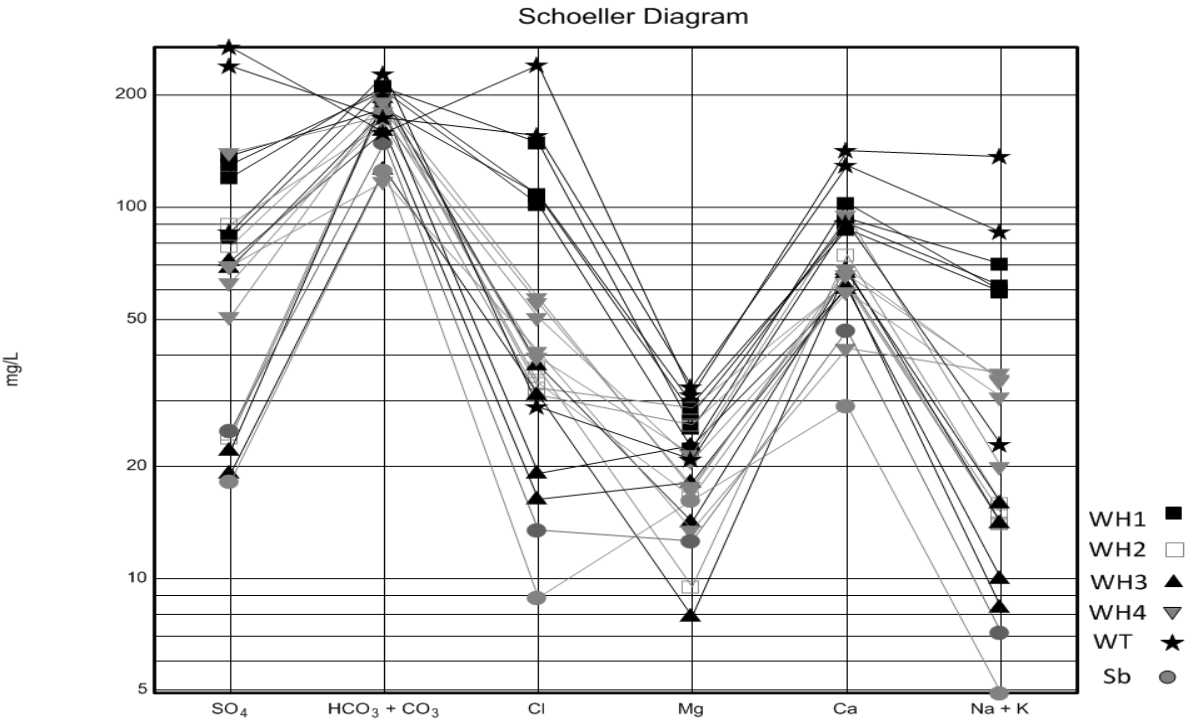

256

Figure 5. Schuler diagram for water samples in the study area 257

3.4. Dominant geochemical processes in water resources of the study area

In general, chemical processes occur during the interaction of water and rock, including dissolution, deposition, oxidation and reduction reactions, and ion exchange. Understanding the hydrogeochemical processes between groundwater and aquifer constituents therefore plays an important role in the analysis of groundwater quality assesement in an area. Composite graphs, ion exchange graphs, and ion ratios are commonly used to study the geochemical processes in a region.

3.5. Composite diagrams

Composite diagrams are used to determine the source of water and the mixing of water from different sources in the water supply. Figure. 6 presents the composite diagram of Ca^{2+}, Mg^{2+}, Na^{+}, HCO_3^{2-}, SO_4^{2-}, Cl^{-} versus total density of soluble ion*s* (TDI). The good correlation of Na^{+}, Cl^{-} and SO_4^{2-} ions with TDI indicates the effect of salinity and solute sources resulting from dissolution of evaporate formations on water quality in the study area. The increasing trend of the Ca^{2+} cation concurrent with the increase in TDI was also due to the correlation of Mg^{2+} with TDI resulting from dissolution of carbonate minerals including calcite and dolomite in the Asmari calcareous formation (As). Figure 7 shows the composite diagram of Ca^{2+}, Na^{+}, HCO_3^{2-}, SO_4^{2-} versus Cl^{-} ions.

Examination of Na^{+} vs. Cl^{-} diagrams as well as Ca^{2+} versus SO_4^{2-} diagrams showed that the dissolution of gypsum and halite in the area was effective on the water quality of the aquifer. However, the good correlation of calcium cation with chlorine anion revealed that the increase in Cl^{-} was not only influenced by the dissolution of these minerals, but other factors also contributed to changes occurred in the area. This can also be seen in the Ca^{2+} diagram against SO_4^{2-} (Fig. 8). In this graph, the molar concentration of calcium is much higher than the molar concentration of sulfate, so the distribution of data in this graph is not on a one-to-one basis in terms of molar ratio. The distribution of samples on all composite diagrams revealed that the presence of elements such as Cl^{-}, Ca^{2+} and SO_4^{2-} in the water resources of the area were likely due to several sources, including dissolution of carbonates, dissolution of gypsum and anhydrite as well as mixing with oil brine.

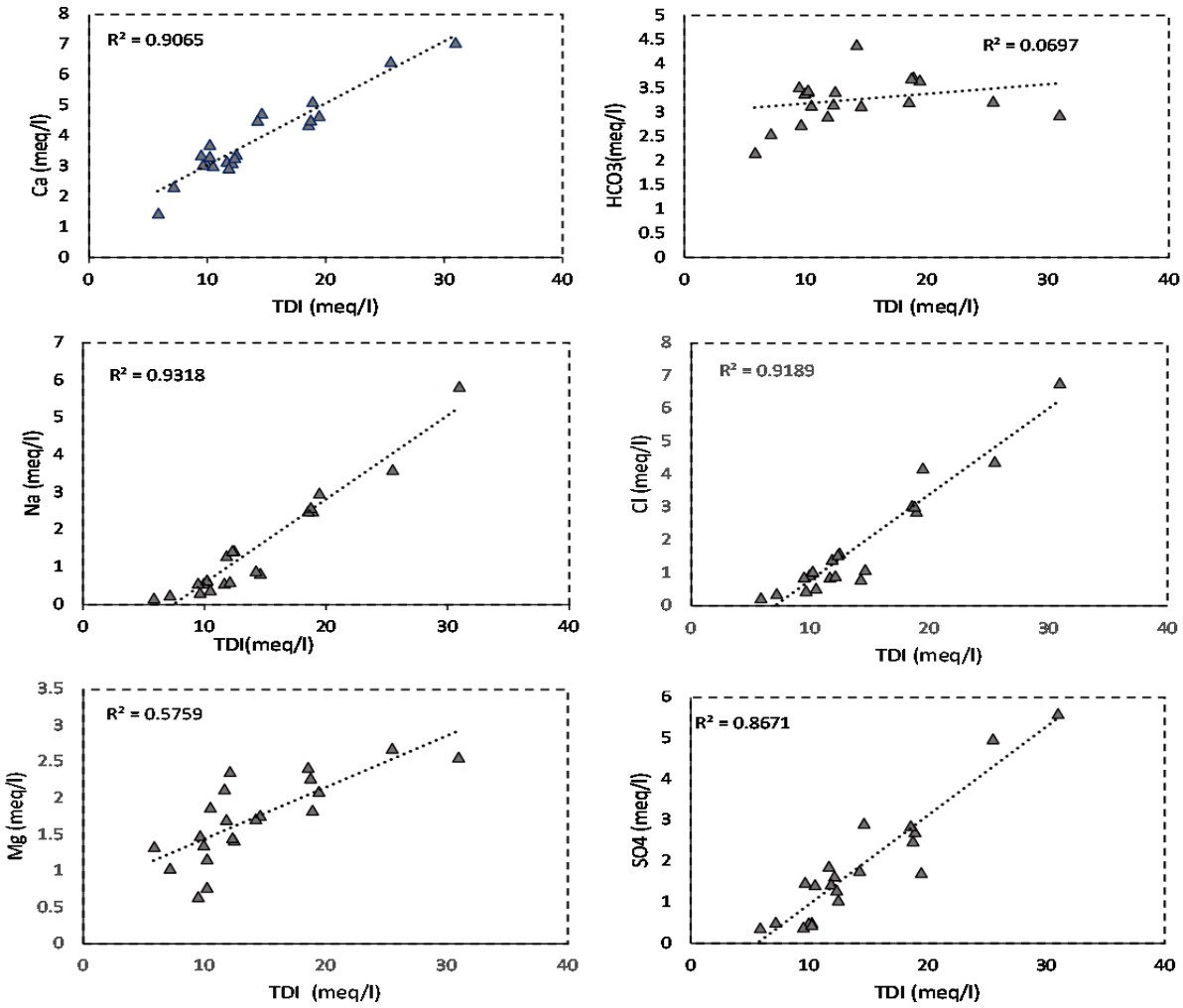

Figure 6. Composite diagrams of the major ions in the samples versus TDI

3.6. Ion Exchange Charts

Ion exchange is generally used to express the processes of transfer of ions from the solid phase (minerals) to the soluble phase (water). If the ion exchange is direct, the sodium and potassium in the soil are replaced with calcium and magnesium in the water; while if reversed, the calcium and magnesium in the soil are replaced with sodium and potassium in the water (ion exchange photo) (equation 4).

Ion exchange is possible in aquifers containing montmorillonite clay. Under these conditions, calcium and magnesium are removed from the water and replaced by sodium. In the reverse ion exchange process, free calcium and sodium are replaced by oil brine or seawater.

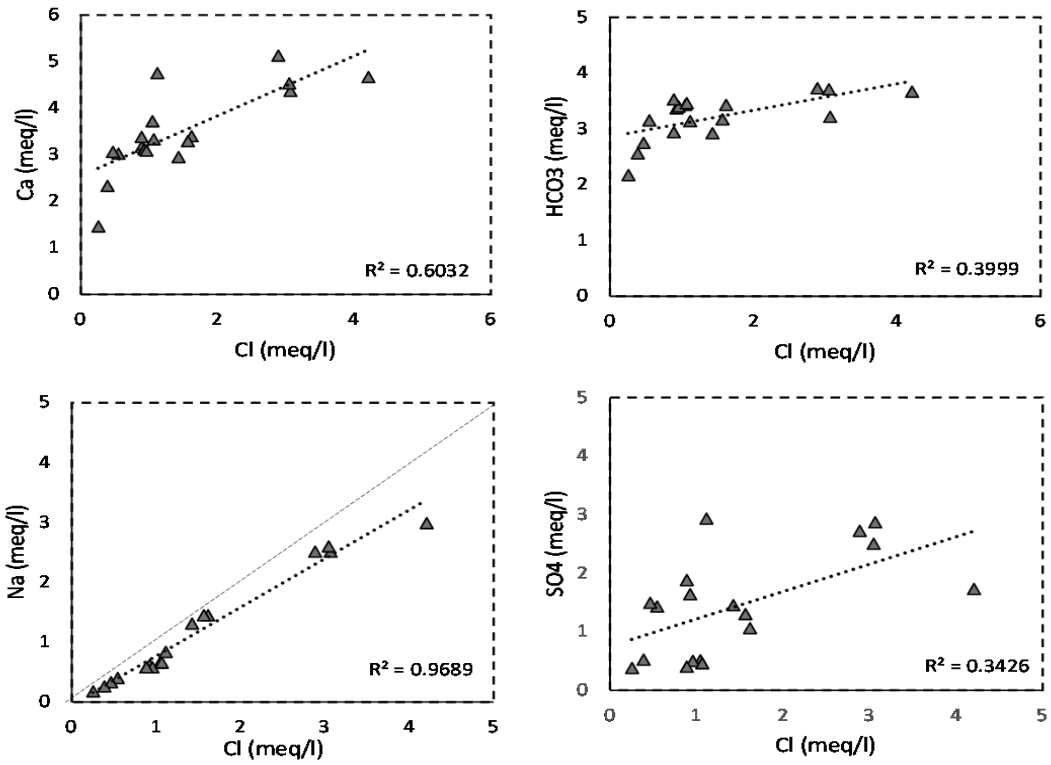

Figure 7. Composite diagram of the major ions versus the chlorine ions

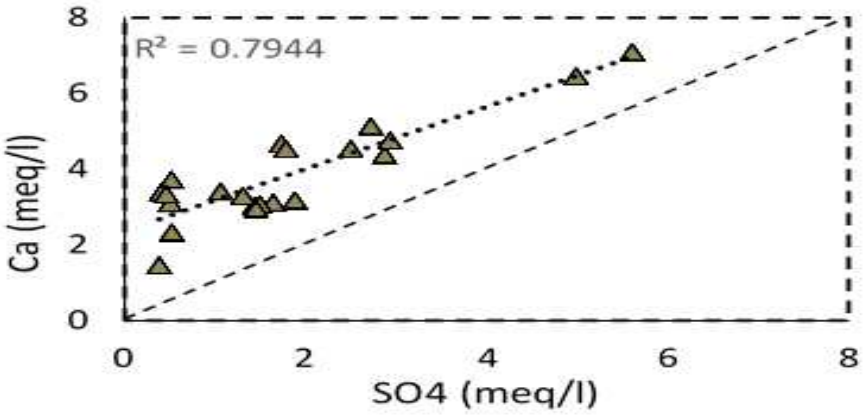

Figure 8. Composite diagram of Ca^{2+} versus SO_4^{2-}

3.7. Calcium Chart (Ca^{2+}) vs. bicarbonate (HCO_3^{2-})

The distribution of points on the equilibrium line (1: 1) shows the dissolution of carbonates (calcite), while the points below the equilibrium line indicate the presence of more bicarbonate than the calcium affected by the calcium outflow resulting from deposition or ion

exchange. The upper points of the equilibrium line also indicate the process of reverse ion exchange and calcium entry from sources other than carbonate minerals including mixing with brine. Examination of Calcium Chart (Ca^{2+}) vs. bicarbonate (HCO_3^{2-}) showed that the bulk distribution of samples on the equilibrium line was also in the upper part of the line, indicating the dissolution of carbonate minerals for the data on the equilibrium line, and the reverse ion exchange for the samples in the upper part of the line, especially the WH1 and WT samples (Fig. 9).

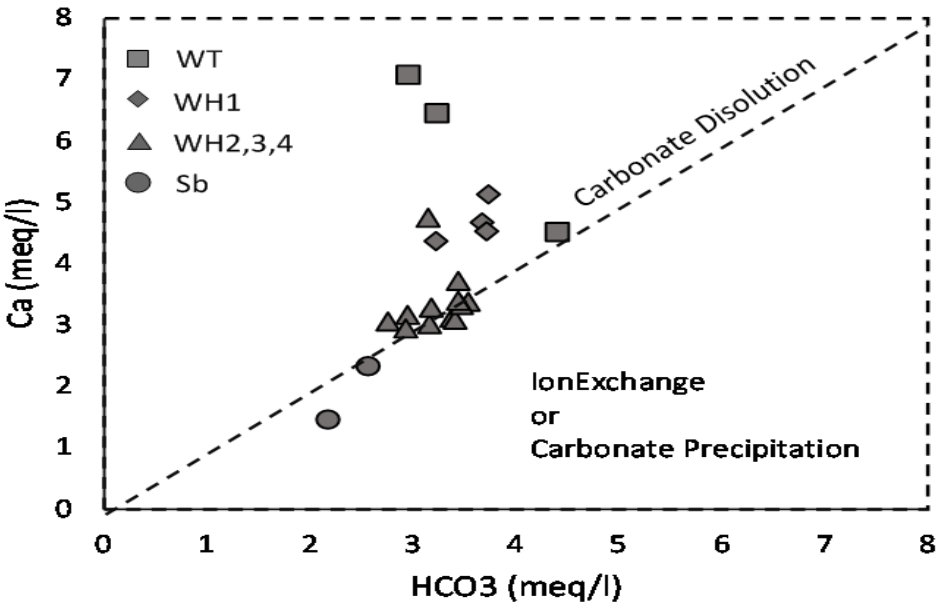

Figure 9. Ion exchange diagrams. Diagram of Ca^{2+} vs. HCO_3^{2}

3.8. Diagram of $Ca^{2++}Mg^{2+}$ vs. $HCO_3^{2-} + SO_4^{2-}$

In the process of analyzing this graph, samples along the equilibrium line (1: 1) showed the dissolution of calcite, dolomite and gypsum. The presence of samples above the equilibrium line indicated the occurrence of inverse ion exchange in these samples. Examination of the sample distribution shows (Fig. 10) that the dominant process in this graph was the reverse ion exchange. In turn, the imbalance of the ratio of sulfate and bicarbonate dissolution to calcium and magnesium suggested that dissolution of carbonate minerals (such as calcite and dolomite) and dissolution of gypsum were not the only sources of calcium supply in these sources. The increase in the two cations mentioned in WT and WH1 was found to be greater than that of other sources (Fig. 11).

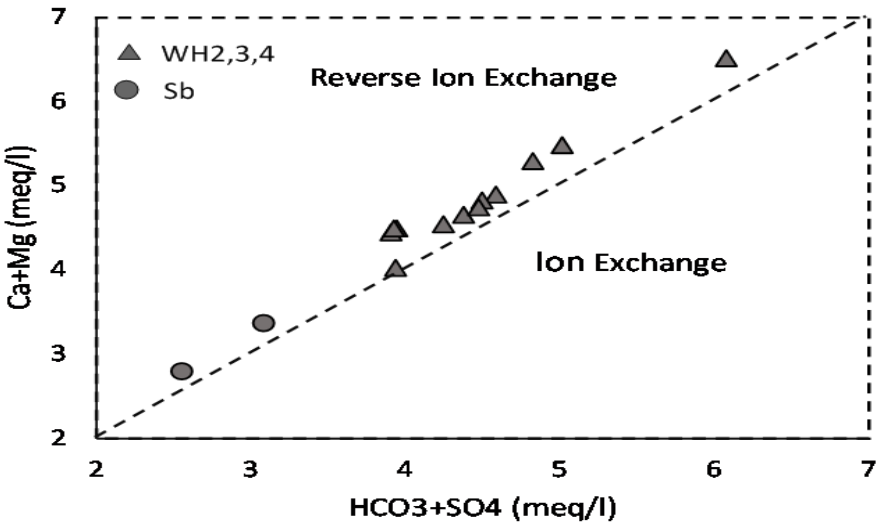

Figure 10. Diagram of $Ca^{2++}Mg^{2+}$ vs. $HCO_3^{2-} + SO_4^{2-}$ for WH2, WH3, WH4, Sb

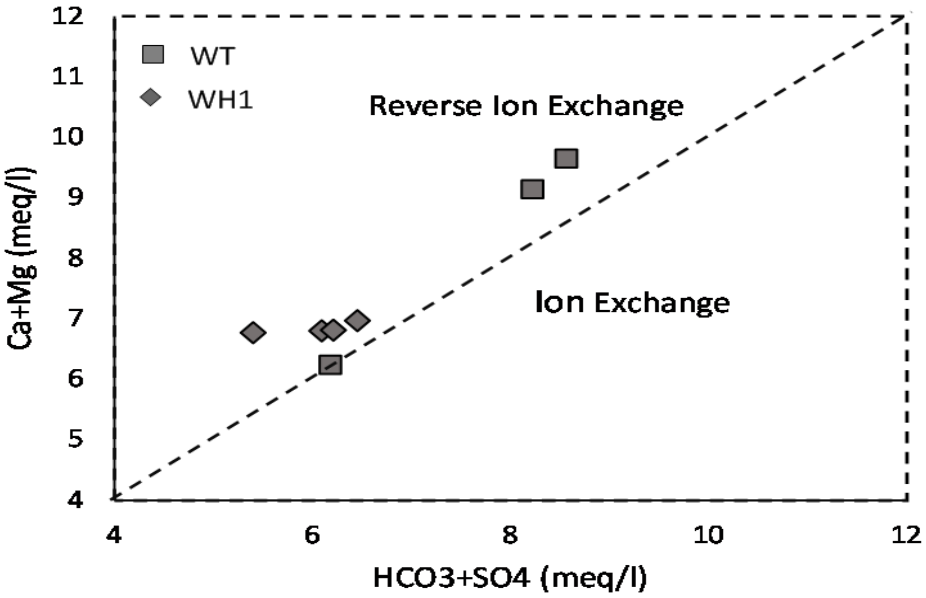

Figure 11. Diagram of $Ca^{2++}Mg^{2+}$ vs. $HCO_3^{2-} + SO_4^{2-}$ for WH1, WT

3.9. Diagram of $Na^{+} + k^{+}$ -Cl^{-} vs. $HCO_3^{2-}+SO_4^{2-}$ -Ca^{2+}-Mg^{2+}

The distribution of the data in the Na + k-Cl diagram vs. Ca + Mg-HCO_3-SO_4 showed that these data were in the upper part of the 1: 1 line and in the reverse ion exchange limit (Fig. 12). The positioning of the data in the negative part of the horizontal axis indicated a higher concentration of chlorine than sodium, while the distribution in the positive part of the

vertical axis was due to the higher concentration of calcium and magnesium compared to sulfate and bicarbonate. Investigating the causes of this distribution, it can be said that dissolution of halite, gypsum and carbonate minerals alone did not increase the concentration of chlorine, calcium and magnesium in comparison with sodium, sulfate and bicarbonate in the water resources of the region. The increase in the concentration of these ions can be due to inputs from other sources such as brine or due to ion exchange.

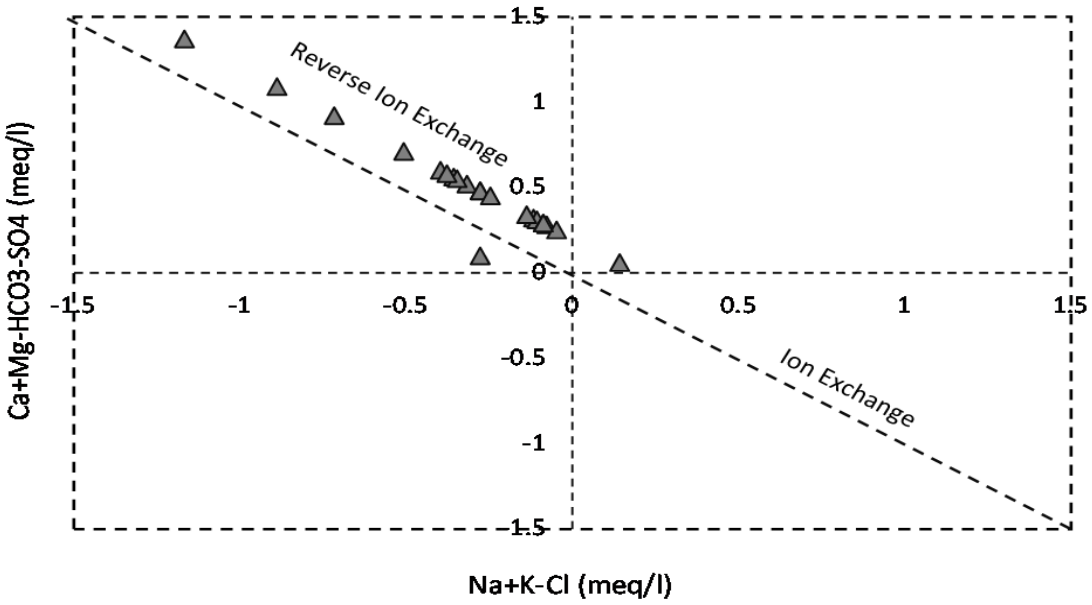

Figure 12. Diagram of $Na^{+}+k^{+}-Cl^{-}$ vs. $HCO_3^{2-}+SO_4^{2-}-Ca^{2+}-Mg^{2+}$

3.10. Na/Cl diagram vs. EC

The ratio of sodium to chlorine is in the Na/Cl diagram versus the vertical axis EC. In the case of halite dissolution, this ratio is one and the data are on the line. The samples above the line are affected by ion exchange, while for the samples in the bottom line the reverse ion exchange occurs (Glover et al. 2012; Jankowski and Acworth 1997). Based on this graph, most of the groundwater samples in the study area are in the reverse ion exchange range (Fig. 13).

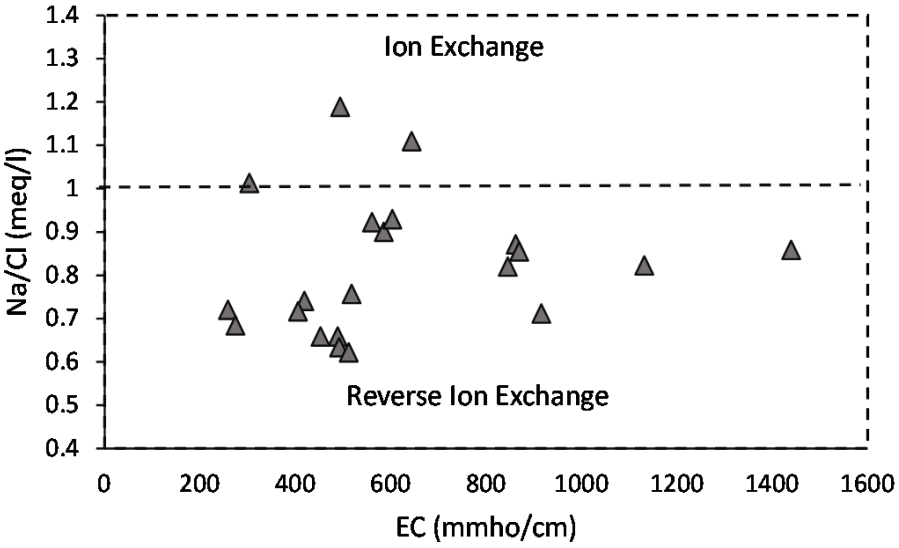

Figure 13. Na/Cl diagram vs. EC

3.11. Ionic ratios of source rock determination

Ionic ratios are appropriate references for ground water hydrochemical studies to determine the source of solutes. These ratios are influenced by the chemical composition of the water-soluble minerals, and the amount of dissolved minerals are of the next importance. The existence of several different sources for one ion or the chemical changes and interactions occurring due to the presence of different compounds and ions are deemed to cause further complexity and deviation of the ion ratios from their theoretical values (Hounslow 1995). To determine the reference ionic ratios and the source of the minerals as well as their relationship with the geological formations, the hydrochemical data were analyzed according to the Hounslow method, 1995 (Tables 2, 3 and 4).

Table 2. Determination of source rock using ion ratios (Hounslow. 1995)

$\frac{Na}{Na+Cl}$	>0.5	Sodium Source other than Halite-albite,Ion Exchange
	=0	Halite Solution
	<0.5 TDS>500	Reverse Softening, Seawater
	<0.5 TDS<500>50	Analysis Error
	<0.5 TDS<50	Rainwater
$\frac{Ca}{Ca+SO_4}$	=0.5	Gypsum dissolution
	<0.5 Ph<5.5	Pyrite Oxidation
	<0.5 Ph Neutral	Calsium removal-IonExchange or Calcite precipitation
	>0.5	Calsium Source other than Gypsum, Carbonate or Silicates
$\frac{Mg}{Mg+Ca}$	=0.5	Dolomite weathering
	<0.5	Limestone-Dolomite weathering
	>0.5	Dolomite dissolution, Calcite precipitation or Sea water

$\frac{Cl}{Sum\ Anion}$	>0.8 TDS>500	Seawater or brine or evaporates
	>0.8 TDS<100	Rainwater
	<0.8	Rock weathering
$\frac{HCO_3}{Sum\ Anion}$	>0.8	Silicate or Carbonate weathering
	<0.8 Sulfate high	Gypsum dissolution
	<0.8 Sulfate low	Seawater brine

368

Table 3. Calculated values of reagent ion ratios (Hounslow. 1995) 369

$\frac{Na}{Na+Cl}$	$\frac{Mg}{Ca+Mg}$	$\frac{Ca}{Ca+SO_4}$	$\frac{Ca+Mg}{SO_4}$	$\frac{Cl}{Sum\ Anion}$	$\frac{HCO_3}{Sum\ Anion}$	نام منبع آب
0.53	0.28	0.72	3.51	0.12	0.63	WT-69
0.45	0.29	0.56	1.83	0.35	0.26	WT-97
0.46	0.27	0.56	1.72	0.44	0.19	WT-104
0.47	0.26	0.65	2.56	0.31	0.40	WH1-07-17
0.45	0.36	0.60	2.37	0.33	0.35	WH1-09-17
0.42	0.31	0.73	3.91	0.44	0.38	WH1-04-18
0.46	0.33	0.64	2.72	0.33	0.40	WH1-05-18
0.40	0.40	0.63	2.82	0.15	0.52	WH2-07-17
0.40	0.43	0.66	3.35	0.16	0.57	WH2-09-17
0.39	0.17	0.88	8.82	0.21	0.69	WH2-04-18
0.38	0.31	0.86	8.90	0.20	0.70	WH2-05-18
0.43	0.38	0.68	3.43	0.11	0.62	WH3-07-17
0.42	0.33	0.67	3.05	0.10	0.59	WH3-09-17
0.40	0.16	0.89	10.08	0.18	0.73	WH3-04-18
0.38	0.26	0.88	9.78	0.21	0.69	WH3-05-18
0.43	0.27	0.62	2.23	0.15	0.44	WH4-07-17
0.48	0.37	0.67	3.21	0.25	0.50	WH4-09-17
0.47	0.30	0.76	4.56	0.26	0.56	WH4-04-18
0.48	0.31	0.72	3.65	0.26	0.53	WH4-05-18
0.41	0.31	0.82	6.48	0.11	0.74	Sb-07-17
0.42	0.48	0.79	7.37	0.09	0.78	Sb-09-17

370

Table 4. Analysis of ion ratios calculated for the study area based on (Hounslow, 1995) 371

$\frac{Na}{Na+Cl}$	<0.5 TDS>500	Reverse ion exchange occurred
$\frac{Ca}{Ca+SO_4}$	>0.5	There is a source other than dissolution of gypsum, carbonates and silicates for calcium ions in these sources.
$\frac{Mg}{Mg+Ca}$	<0.5	Weathering of calcite and dolomite
$\frac{Cl}{Sum\ Anion}$	<0.8	Weathering of stone
$\frac{HCO_3}{Sum\ Anion}$	<0.8	dissolution of gypsum

372

Analysis of the ionic ratios of sodium and chlorine indicated a reverse ion exchange in the region. These ratios for calcium and sulfate revealed that dissolutions of gypsum, carbonates 373 374

and silicate minerals were not the only source of calcium in these sources. Weathering of calcite and dolomite as well as dissolution of gypsum in the water resources in the region were other results of ion ratios analysis.

3.12. Diagram of salinity source assessment

Na/Cl ratio

Na/Cl weight ratio was used to separate halite dissolution from oilfield brine. If the Na/Cl weight ratio was between 0.63 and 0.65, the salinity factor was due to the dissolution of halite which, if less than 0.6, showed the mixing of water with oil brine (Leonard and Ward 1962). Investigation of sodium to chlorine ion ratio in the study area showed that in most of the samples the weight ratio was less than 0.6 (Table 5). Investigation of this ratio in Atabaki well revealed that at 69 m depth WT, the values of Na^+ and Cl^- were approximately equal. It was also found that with increasing depth (97 and 104 m depth), the difference in concentration of two ions increased due to the increase of Cl^-ion concentration. This, in turn, shows the probable mixing of water wells with oil brine at lower depths of this aquifer.

Table 5. Na/Cl weight ratio

Na/Cl(mg/l)	Water resources	Na/Cl(mg/l)	Water resources
0.6	WH4-05-18	0.42	WH2-07-17
0.56	WH1-07-17	0.43	WH2-09-17
0.53	WH1-09-17	0.41	WH2-04-18
0.46	WH1-04-18	0.39	WH2-05-18
0.55	WH1-05-18	0.48	WH3-07-17
0.71	WT-69	0.46	WH3-09-17
0.53	WT-97	0.42	WH3-04-18
0.55	WT-104	0.4	WH3-05-18
0.44	Sb-07-17	0.49	WH4-07-17
0.46	Sb-09-17	0.59	WH4-09-17
		0.58	WH4-04-18

Figure 14 shows the samples studied in the diagram of Na/Cl weight ratio versus Cl^-. The distribution of data in this graph is in the range of mixing of freshwater with oil brine.

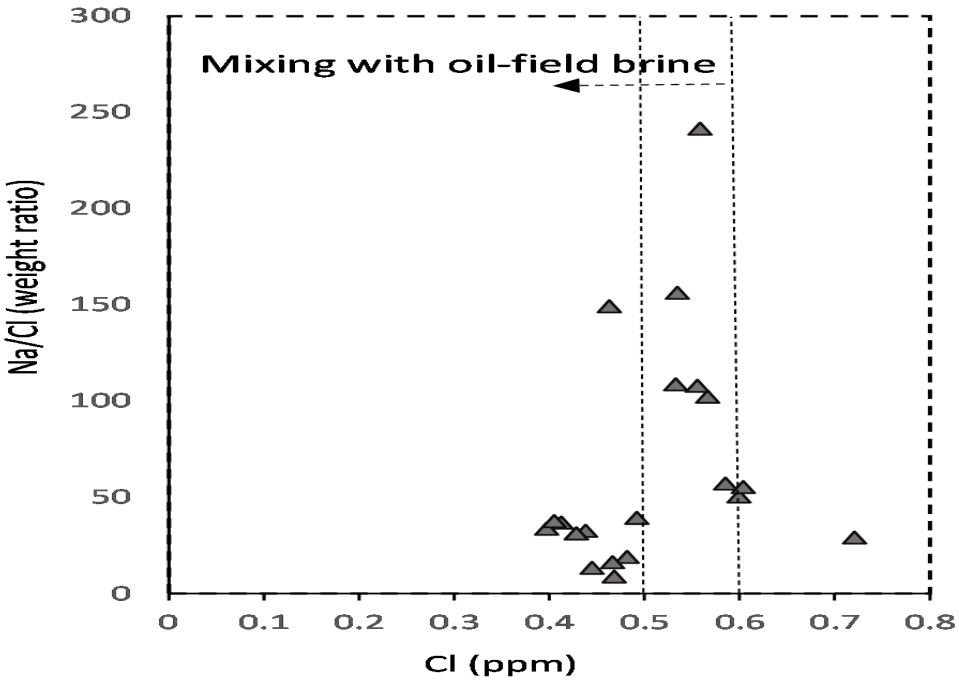

Figure 14. The graph of the Na/Cl ratio versus Cl^- in terms of weight ratio

In sodium vs. chlorine diagrams in terms of mole ratio, if the samples were below the halite dissolve line (HDL) and deep water mixing line (DWML), the Cl-ion concentration was higher than Na^+. Mixing with brine may be the cause for the difference in ratios. In turn, examination of the samples in the chlorine versus sodium diagrams showed that WH1, WH2, WH3, and the WH4 July sample were below the DWML line, indicating the mixing of oil brine with the freshwater sources available (Figures 15 and 16).

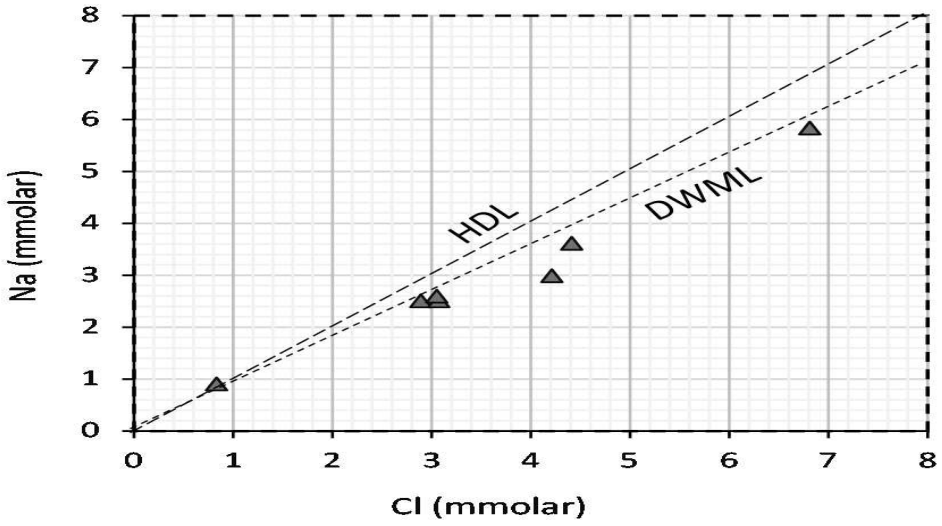

Figure 15. Diagram of Na^+ ratio to Cl^- of WT and WH1 samples

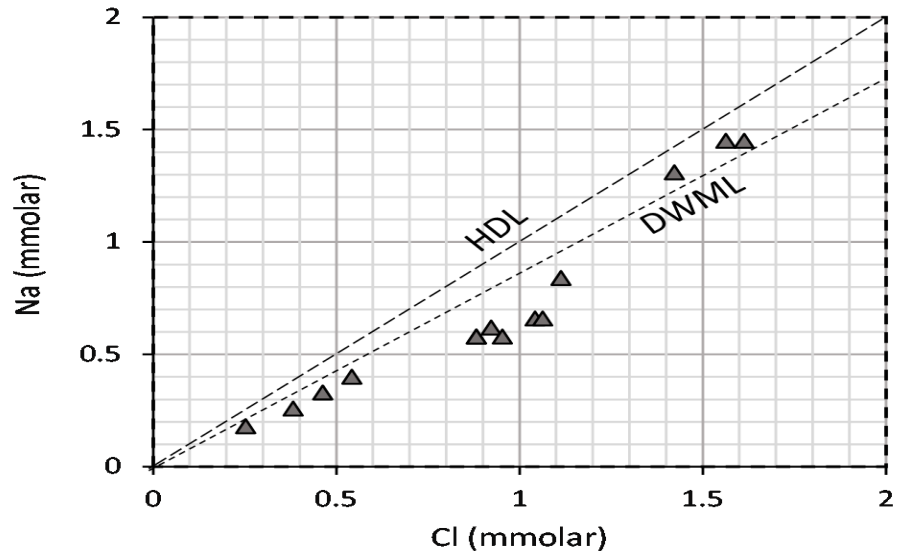

Figure 16. The graph of the Na^+ ratio to Cl^- of samples in WH2, WH3, WH4, Sb

3.13. (Ca + Mg) / SO4 vs. Na/Cl

In evaporate formations, halite minerals are often associated with gypsum and anhydrite. In the case of dissolution of evaporate minerals, the molar ratio of calcium to sulfate and sodium to Cl^- is equal to one (Richter and Kreitler 1991). Implementation of the data gathered from the study area on the $(Ca+Mg)/SO_4$ diagram vs. Na/Cl showed that the molar ratio $(Ca+Mg)/SO_4$ was higher than one, while the Na/Cl molar ratio was lower than one (Fig. 17). This indicates that samples are in the mixing range with oil brine.

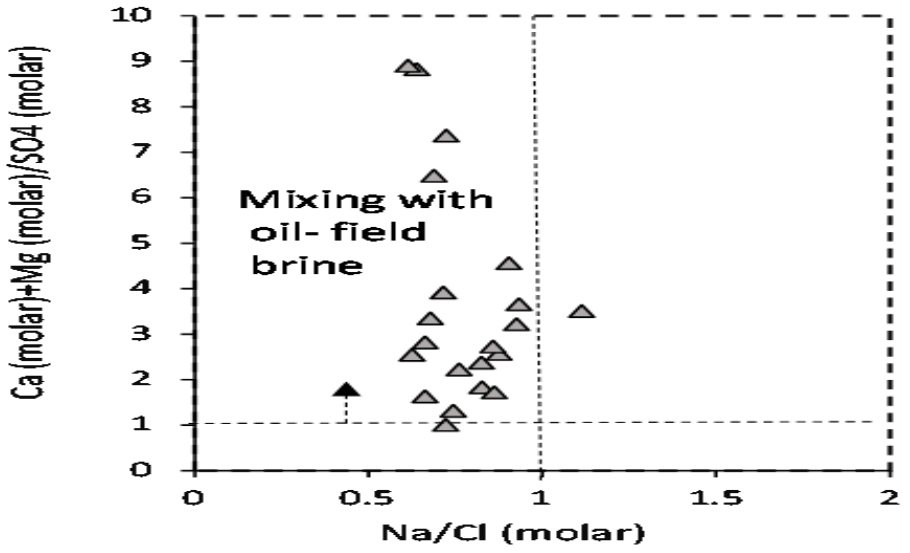

Figure 16 (Ca + Mg) / SO4 diagram vs. Na/Cl

3.14. SO4/Cl diagram vs. Cl

The SO_4/Cl ratio is used as an indicator to detect the mixing of freshwater with oil brine (Rouhi and Kalantari 2018; Whittemore and Pollock 1979). The representation of data on the SO_4/Cl ion ratio versus Cl^- in terms of weight ratio showed that the data fell within the mix of freshwater with oil brine (Fig. 18).

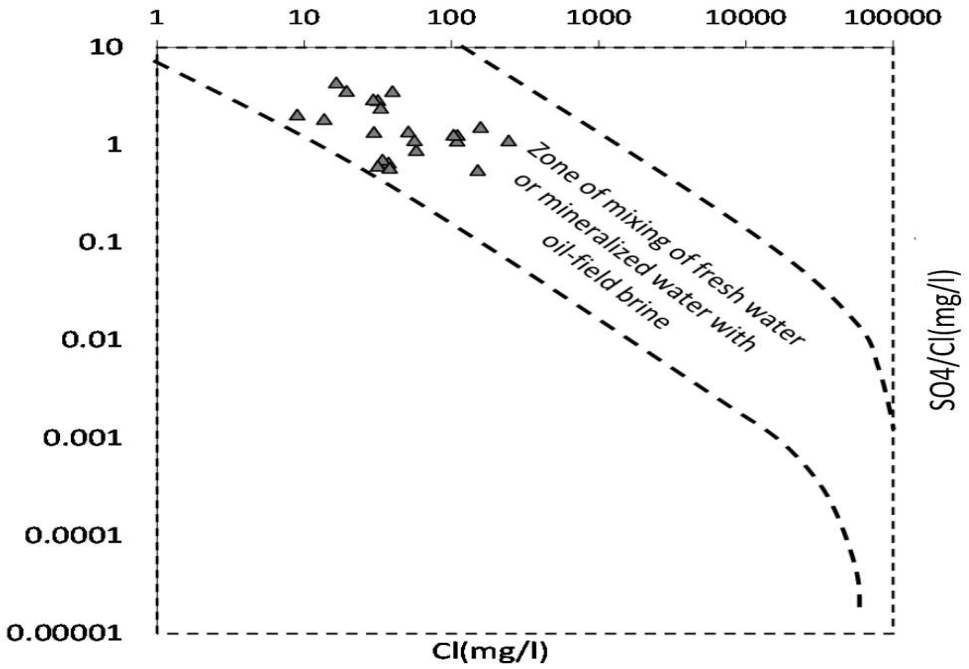

Figure 18. Diagram of the ion ratio of SO_4/ Cl to Cl^- in terms of weight ratio

3.15. Br/Cl and I/Cl ratios

Br^- and I^- are used as the most important elements in the investigation of groundwater mixing with hydrocarbon brine (Han et al. 2014; Kumar et al. 2015). There is a large difference between the concentration of these elements in oil brine and brine from dissolution of halite (Freeman 2007). Throughout this study, different techniques were used for hydrogeochemical investigation of the origin of the qualitative changes in the region. In all the studies, reverse ion exchange and infiltration of deep brine with high amounts of calcium and chlorine were identified as the factors changing the water quality. As the study area is adjacent to the oil reservoirs, the concentration of Br^- and I^- ions and their ratios to Cl^- ions was measured in order to investigate the mixing of hydrocarbon brine with water resources in the region more accurately (Table 6). Waters with a bromine/chlorine ratio of more than 1×10^{-3} were identified as the salinity factor, and the increase in their chlorine content was found to be due

to their mixing with the brine of the oil fields in the region (Cartwright et al. 2006; Whittemore and Pollock 1979).

Table 6. Br/Cl and I/Cl ratios

I/Cl Mg/l	Br/Cl Mg/l	Water resources
0.0013	0.028	**WH2-05-18**
0.00084	0.0172	**WH3-05-18**
0.0014	0.0141	**WH4-05-18**
0.0032	0.0091	**WH1-07-17**
0.00011	0.0057	**WH1-09-17**
0.00017	0.00686	**WH1-09-18**
0.000074	0.020	**WT-104**

Examination of the ratio of these elements in the studied water samples showed that all samples were affected by the influence of oil brine. The use of the Br/Cl ratio diagram versus chlorine also showed the distribution of these data in the range of oil-brine mixing zones (Fig. 19).

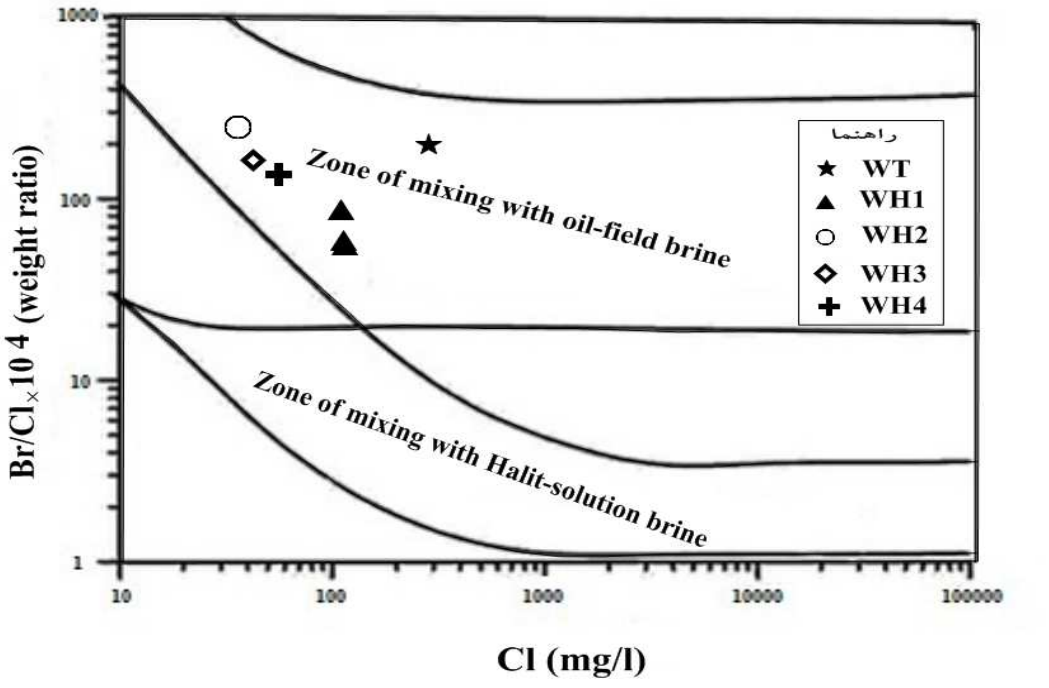

Figure 19. Br/Cl ratio diagram versus Cl in weight ratio

3.16. Total Organic Carbon

Total organic carbon is an indicator for detecting contamination of water resources with organic matter. If the concentration of TOC in water is more than 2 mg/lit, it indicates contamination with hydrocarbons (Chitsazan et al. 2017; Spruill 1988). TOC index was used to study the penetration of hydrocarbons in the region's water resources. The TOC analysis in the WT sample showed that the concentration of this parameter is 23.2 mg/L, indicating the penetration of hydrocarbon materials into this source.

3.17. Sulfur

As one of the main problems in the development of Kamarderaz anticline aquifer is the outflow of H_2S and the bad smell of water coming out of the wells in the area, the factors related to this phenomenon were studied in the region. Sulfur is the tenth most abundant element in the world and the 14th most abundant in the Earth's crust. Therefore, it is possible to know the origin of minerals containing sulfur and its derivatives by using sulfur isotopes (Seal 2006). Elemental sulfur can be deposited as a yellow sediment as a result of H_2S emissions.

Analysis of the 104m depth sample of WT showed high levels of elemental sulfur (78.98 mg/l) in the water of this well. Therefore, to investigate the involvement of hydrocarbons in the production of H_2S gas and the deposition of sulfur in this well, the analysis of δ^{34}s isotope in sulfate was performed on the water sample of the well. The sulfur isotope content in this study was estimated to be +19.3 per thousand. According to the region's formations and the results of sulfur isotope analysis as well as elemental sulfur, various mechanisms were identified for H_2S production in the region, including bacterial sulfate reduction, thermochemical sulfate reduction, and the contact of anhydrite with hydrocarbon materials.

Thermochemical reduction of sulfate in deep carbonate reservoirs was identified to play an important role in H_2S production (Saberi 2019; Worden and Smalley 1996). This process occurs at temperatures above 127 °C. In this process, sulfur and H2S gas are produced by the reaction of anhydrite and hydrocarbon (Eq. 3). In addition to the thermochemical reduction of sulfate, water-soluble sulfate can produce H_2S gas by a bacterial sulfate reduction process at temperatures below 80°C (Eq. 4) (Heydari 1997; Khatib and Salanitro 1997). Other mechanisms of H_2S production include the contact of hydrocarbons with sulfated layers such as anhydrite or gypsum in the formation and in the process of bacterial reduction of H_2S gas

production (Eq. 5). In this mechanism, sulfate reducing bacteria derive their energy from organic matter. The requirements for bacterial sulfate reduction are low salinity, high sulfate, high TOC, and neutral pH (Saberi 2019; Teske et al. 1998). At low temperatures, thermal decomposition of sulfur organic compounds in the early stages of oil maturity is another process that produces a moderate H_2S concentration (Martins and Marques 2006). Isotopic studies show that the isotope range of $\delta^{34}S$ in sulfate in evaporate minerals such as gypsum and anhydrite is + 10- + 30 per thousand (Claypool et al. 1980; Worden and Smalley 1996; Zega et al. 2015). Therefore, the source of sulfate in the Kamarderaz anticline water resources is probably the gypsum and anhydrite minerals in the Gs and As formations, producing H_2S gas in the presence of hydrocarbon materials, and under the influence of one of the above processes.

$$2CaSO_4+C_2H_6 \rightarrow 2CaCO_3+S+H_2S+2H_2O \quad (3)$$

$$SO_4(aq)+Hydrocarbone \rightarrow H_2S+CO_2+CaCO_3 \quad (4)$$

$$SO_4(solid)+Hydrocarbone \rightarrow H_2S+CO_2+H_2O \quad (5)$$

4. Conclusions

Applying the results of chemical analysis of the samples in the Piper and Durov diagrams showed that the dominant water type was Ca-HCO_3, and in WT and WH1 the water type changed from Ca-HCO_3 to Ca-Cl. Besides, the distribution of samples in all composite diagrams showed that the presence of elements such as Cl^-, Ca^{2+} and SO_4^{2-} in water resources in the study area was probalby due to several sources including dissolution of carbonates, gypsum and anhydrite as well as mixing with brine. Ion exchange diagrams in the region's water resources also revealed that most samples examined in the study area fell within the reverse ion exchange range. Analysis of the ionic ratios of sodium and chlorine also indicated a reverse ion exchange in the region. In turn, these ratios for calcium and sulfate showed that gypsum dissolution and carbonate dissolution were not the only sources of calcium supply in these sources. The analysis results of salinity source diagrams in the study area confirmed the interaction of oil brine with the water resources in the region. Br/Cl, I/Cl ion ratios and Cl-Br/Cl diagrams as the most important elements and ratios in the investigation of groundwater mixing with oil brine revealed that all investigated water sources were subject to contamination with oil brine. Moreover, TOC analysis on the WT sample revealed the presence of hydrocarbon materials in the well indicating the impact of the region's oil reservoirs on the karstic sources of the anticline. Additionally, the results of elemental sulfur

and isotope $\delta^{34}S$ in sulfate showed that the mechanism of bacterial reduction of water-soluble sulfate or sulfate present in evaporate minerals was more likely to produce H_2S gas in the presence of hydrocarbons in the region. To conclude, the results of different hydrochemical investigations in this study showed that the low water quality of Kamarderaz anticline plunge water resources was affected by the solute inflow from Gachsaran evaporate formation and also the infiltration of oil brine in the region into the groundwater resources.

Conflict of Interests

Authors have no conflict of interests.

Acknowledgments

The authors are to acknowledge the Department of Geology, Faculty of Earth Science, Shahid Chamran University of Ahvaz, Ahvaz, Iran for their cooperation in obtaining the required data.

Disclosure statement

No potential conflict of interest was reported by the authors.

-Ethical Approval

This study was originally approved by the Shahid Chamran University of Ahvaz, Ahvaz, Iran.

-Consent to Participate

'Not applicable' for that specific section.

-Consent to Publish

'Not applicable' for that specific section.

-Authors Contributions

Study concept, design and critical revision of the manuscript for important intellectual content: Seyed Yahya Mirzaee Aranki, Sorour Mazrae asl, Hosein Karimi Vardanjani drafting of the manuscript and advisor: Seyed Yahya Mirzaee Aranki; performing the experiments Seyed Yahya Mirzaee Aranki, Sorour Mazrae asl.

-Funding

This work was financially supported by Shahid Chamran University of Ahvaz, Ahvaz, Iran.

-Competing Interests

persons who meet authorship criteria are listed as authors, and all authors certify that they have participated sufficiently in the work to take public responsibility for the content, including participation in the concept, design, analysis, writing, or revision of the manuscript. The name of each author must appear at least once in each of the three categories below.

Category 1

- Conception and design of study: Seyed Yahya Mirzaee Aranki, Sorour Mazrae asl, Hosein Karimi Vardanjani
- acquisition of data: Seyed Yahya Mirzaee Aranki
- analysis and/or interpretation of data: Sorour Mazrae asl, Hosein Karimi Vardanjani

Category 2

- Drafting the manuscript: Seyed Yahya Mirzaee Aranki, Sorour Mazrae asl, Hosein Karimi Vardanjani
- revising the manuscript critically for important intellectual content: Seyed Yahya Mirzaee Hosein Karimi Vardanjani

Category 3

Approval of the version of the manuscript to be published (the names of all authors must be listed):

Seyed Yahya Mirzaee Aranki, Sorour Mazrae asl, Hosein Karimi Vardanjani

-Availability of data and materials

'Not applicable' for that specific section.

References

Beydoun, Z., Clarke, M. H., & Stoneley, R. (1992). Petroleum in the Zagros basin: a late tertiary foreland basin overprinted onto the outer edge of a vast hydrocarbon-rich paleozoic-mesozoic passive-margin shelf: chapter 11.

Cartwright, I., Weaver, T. R., & Fifield, L. K. (2006). Cl/Br ratios and environmental isotopes as indicators of recharge variability and groundwater flow: an example from the southeast Murray Basin, Australia. *Chemical Geology, 231*(1-2), 38-56.

Chitsazan, M., Shacheri, S., Mirzaee, S., & Aboudi, S. (2017). assessment of karstic aquifer water resources ase study Garuo karstic spring located in eastern of Khuzestan. *journal of Advanced Applied Geology*, 65-75.

Claypool, G. E., Holser, W. T., Kaplan, I. R., Sakai, H., & Zak, I. (1980). The age curves of sulfur and oxygen isotopes in marine sulfate and their mutual interpretation. *Chemical geology, 28*, 199-260.

Dogramaci, S. S., & Herczeg, A. L. (2002). Strontium and carbon isotope constraints on carbonate-solution interactions and inter-aquifer mixing in groundwaters of the semi-arid Murray Basin, Australia. *Journal of Hydrology, 262*(1-4), 50-67.

Fan, Q., Ma, H., Lai, Z., Tan, H., & Li, T. (2010). Origin and evolution of oilfield brines from Tertiary strata in western Qaidam Basin: Constraints from 87 Sr/86 Sr, δD, δ 18 O, δ 34 S and water chemistry. *Chinese Journal of Geochemistry, 29*(4), 446-454.

Fontes, J. C., & Matray, J. (1993). Geochemistry and origin of formation brines from the Paris Basin, France: 2. Saline solutions associated with oil fields. *Chemical Geology, 109*(1-4), 177-200.

ford, & Williams (2007). Karst Hydrogeology and Geomorphology. John Wiley & Sons Ltd, Chichester.

Freeman, J. T. (2007). The use of bromide and chloride mass ratios to differentiate salt-dissolution and formation brines in shallow groundwaters of the Western Canadian Sedimentary Basin. *Hydrogeology Journal, 15*(7), 1377-1385.

Glover, E., Akiti, T., & Osae, S. (2012). Major ion chemistry and identification of hydrogeochemical processes of ground water in the Accra Plains. *Geoscience, 50*, 10279-10288.

Han, D., Song, X., Currell, M. J., Yang, J., & Xiao, G. (2014). Chemical and isotopic constraints on evolution of groundwater salinization in the coastal plain aquifer of Laizhou Bay, China. *Journal of Hydrology, 508*, 12-27.

Heydari, E. (1997). The role of burial diagenesis in hydrocarbon destruction and H2S accumulation, Upper Jurassic Smackover Formation, Black Creek Field, Mississippi. *AAPG bulletin, 81*(1), 26-45.

Hounslow, A. (1995). *Water quality data: analysis and interpretation*: CRC press.

Jalali, M. (2011). Nitrate pollution of groundwater in Toyserkan, western Iran. *Environmental Earth Sciences, 62*(5), 907-913.

Jankowski, J., & Acworth, R. I. (1997). Impact of debris-flow deposits on hydrogeochemical processes and the developement of dryland salinity in the Yass River Catchment, New South Wales, Australia. *Hydrogeology journal, 5*(4), 71-88.

Jean, J.-S., Liao, L., Kar, S., Liu, C.-C., & Li, Z. (2016). Hydrochemistry of hot springs in geothermal fields of central, northern, and northeastern Taiwan: implication on occurrence and enrichment of arsenic. *Environmental Earth Sciences, 75*(19), 1316.

Khatib, Z., & Salanitro, J. Reservoir souring: analysis of surveys and experience in sour waterfloods. In *SPE Annual Technical Conference and Exhibition, 1997*: Society of Petroleum Engineers

Kumar, M., Rao, M. S., Deka, J. P., Ramanathan, A., & Kumar, B. (2015). Integrated hydrogeochemical, isotopic and geomorphological depiction of the groundwater salinization in the aquifer system of Delhi, India. *Journal of Asian Earth Sciences, 111*, 936-947.

Leonard, A., & Ward, P. (1962). Use of Na/Cl ratios to distinguish oil-field from salt-spring brines in western Oklahoma. *US Geological survey professional paper*, B126-8127.

Mahmoudi, N., Nakhaei, M., & Porhemmat, J. (2017). Assessment of hydrogeochemistry and contamination of Varamin deep aquifer, Tehran Province, Iran. *Environmental Earth Sciences, 76*(10), 370.

Martins, M. d. O., & Marques, L. C. d. C. Assessment of Oilfield Souring Mechanisms by Mass Spectrometry Analysis of the Sulfur Isotopes Ratio. In *International Oil Conference and Exhibition in Mexico, 2006*: Society of Petroleum Engineers

Mast, V. A. (1985). The use of ionic mixing curves in differentiating oil field brine from natural brine in a fresh water aquifer. *Groundwater Monitoring & Remediation, 5*(3), 65-69.

Matray, J., Lambert, M., & Fontes, J. C. (1994). Stable isotope conservation and origin of saline waters from the Middle Jurassic aquifer of the Paris Basin, France. *Applied Geochemistry, 9*(3), 297-309.
Mirzaee, S., Chitsazan, M., Karimi, H., & Piri, Z. (2019). Hydrochemical investigations of Sargarou spring Dehloran. *journal of Advanced Applied Geology*.
Panno, S., Hackley, K. C., Cartwright, K., & Liu, C.-L. (1994). Hydrochemistry of the Mahomet Bedrock Valley Aquifer, east-central Illinois: Indicators of recharge and ground-water flow. *Ground Water, 32*(4), 591-605.
Richter, B., & Kreitler, C. (1991). Identification of sources of ground-water salinization using geochemical techniques. US Environmental Protection Agency EPA. *Ada, Okalahoma*.
Rouhi, H., & Kalantari, N. (2018). Hydrogeochemistry and groundwater mixing close to an oil field: an example from Asmari karstic aquifer, Khuzestan, Iran. *Water Science and Technology: Water Supply, 18*(2), 357-370.
Saberi, M. H. (2019). The feasibility of depositing the reservoir into hydrogen-sulfide as a result of EOR process in Cheshm-e Khosh oil field, western Iran. *Arabian Journal of Geosciences, 12*(2), 66.
Sarikhani, R., Dehnavi, A. G., Ahmadnejad, Z., & Kalantari, N. (2015). Hydrochemical characteristics and groundwater quality assessment in Bushehr Province, SW Iran. *Environmental Earth Sciences, 74*(7), 6265-6281.
Seal, R. (2006). Sulfure isotope geochemistry of sulfide minerals. *US Geological survey professional paper*.
Sefie, A., Aris, A. Z., Ramli, M. F., Narany, T. S., Shamsuddin, M. K. N., Saadudin, S. B., et al. (2018). Hydrogeochemistry and groundwater quality assessment of the multilayered aquifer in Lower Kelantan Basin, Kelantan, Malaysia. *Environmental earth sciences, 77*(10), 397.
Sherkati, S., & Letouzey, J. (2004). Variation of structural style and basin evolution in the central Zagros (Izeh zone and Dezful Embayment), Iran. *Marine and petroleum geology, 21*(5), 535-554.
Spruill, T. B. (1988). Use of Total Organic Carbon as an Indicator of Contamination from an Oil Refinery, South-Central Kansas. *Groundwater Monitoring & Remediation, 8*(3), 76-82.
Teske, A., Ramsing, N. B., Habicht, K., Fukui, M., Küver, J., Jørgensen, B. B., et al. (1998). Sulfate-reducing bacteria and their activities in cyanobacterial mats of Solar Lake (Sinai, Egypt). *Applied and Environmental Microbiology, 64*(8), 2943-2951.
Thilagavathi, R., Chidambaram, S., Pethaperumal, S., Chivaya, S., Rao, M., Tirumales, K., et al. (2016).) An attempt to understand the behavior of dissolved organic carbon in coastal aquifers of Pandicherry region. *Environmental Earth Sciences*, doi:10.1007/sl2665-015-48335.
Whittemore, D. O., & Pollock, L. M. (1979). Determination of salinity sources in water resources of Kansas by minor alkali metal and halide chemistry. *Available from the National Technical Information Service, Springfield VA 22161 as PB 80-128911, Price codes: A 03 in paper copy, A 01 in microfiche. Contribution*(208).
Worden, R., & Smalley, P. (1996). H2S-producing reactions in deep carbonate gas reservoirs: Khuff Formation, Abu Dhabi. *Chemical Geology, 133*(1-4), 157-171.
Wurbs, R. A. (2011). Water supply reliability as influenced by natural salt pollution. *Journal of Contemporary Water Research and Education, 106*(1), 15.
Zaporozec, A. (1972). Graphical interpretation of water quality data. *Ground Water, 10*(2), 32-43.
Zarei, M., Raeisi, E., Merkel, B. J., & Kummer, N.-A. (2013). Identifying sources of salinization using hydrochemical and isotopic techniques, Konarsiah, Iran. *Environmental Earth Sciences, 70*(2), 587-604.
Zega, M., Rožič, B., Gaberšek, M., Kanduč, T., Rožič, P. Ž., & Verbovšek, T. (2015). Mineralogical, hydrogeochemical and isotopic characteristics of the Žveplenica sulphide karstic spring (Trebuša Valley, NW Slovenia). *Environmental Earth Sciences, 74*(4), 3287-3300.

Figures

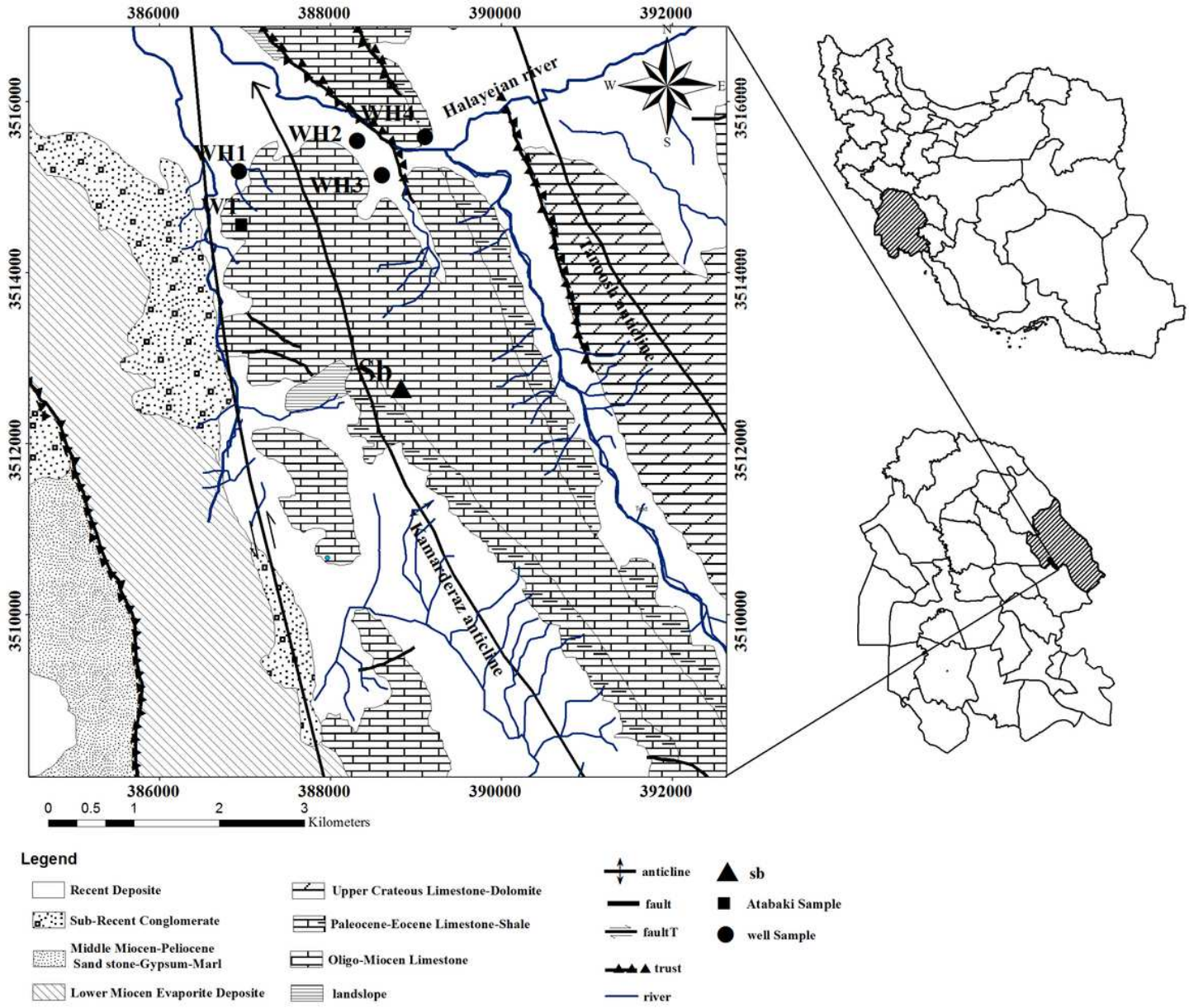

Figure 1

Location map of the study area, sampling sources and formation outcrops in the area using the 1967 Oil Company map. Note: The designations employed and the presentation of the material on this map do not imply the expression of any opinion whatsoever on the part of Research Square concerning the legal status of any country, territory, city or area or of its authorities, or concerning the delimitation of its frontiers or boundaries. This map has been provided by the authors.

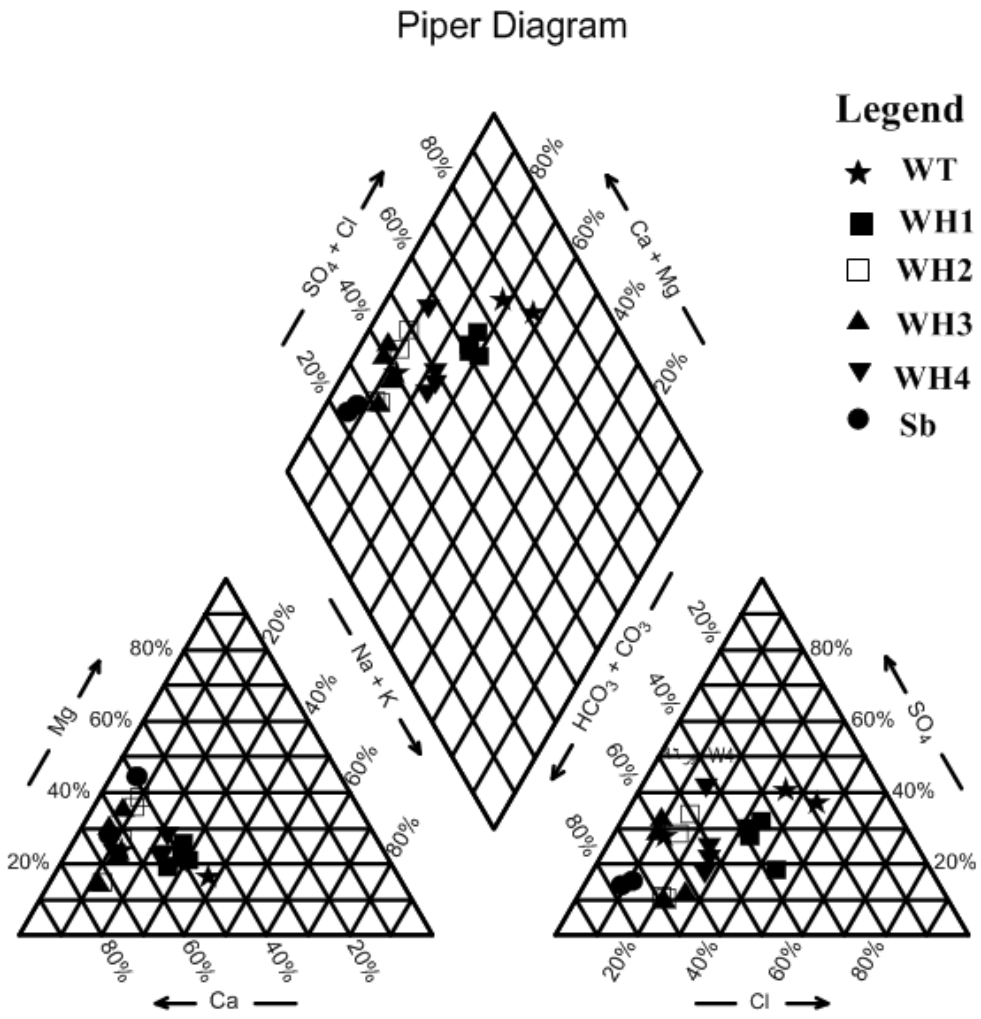

Figure 2

Representation of the studied samples in the Piper diagram

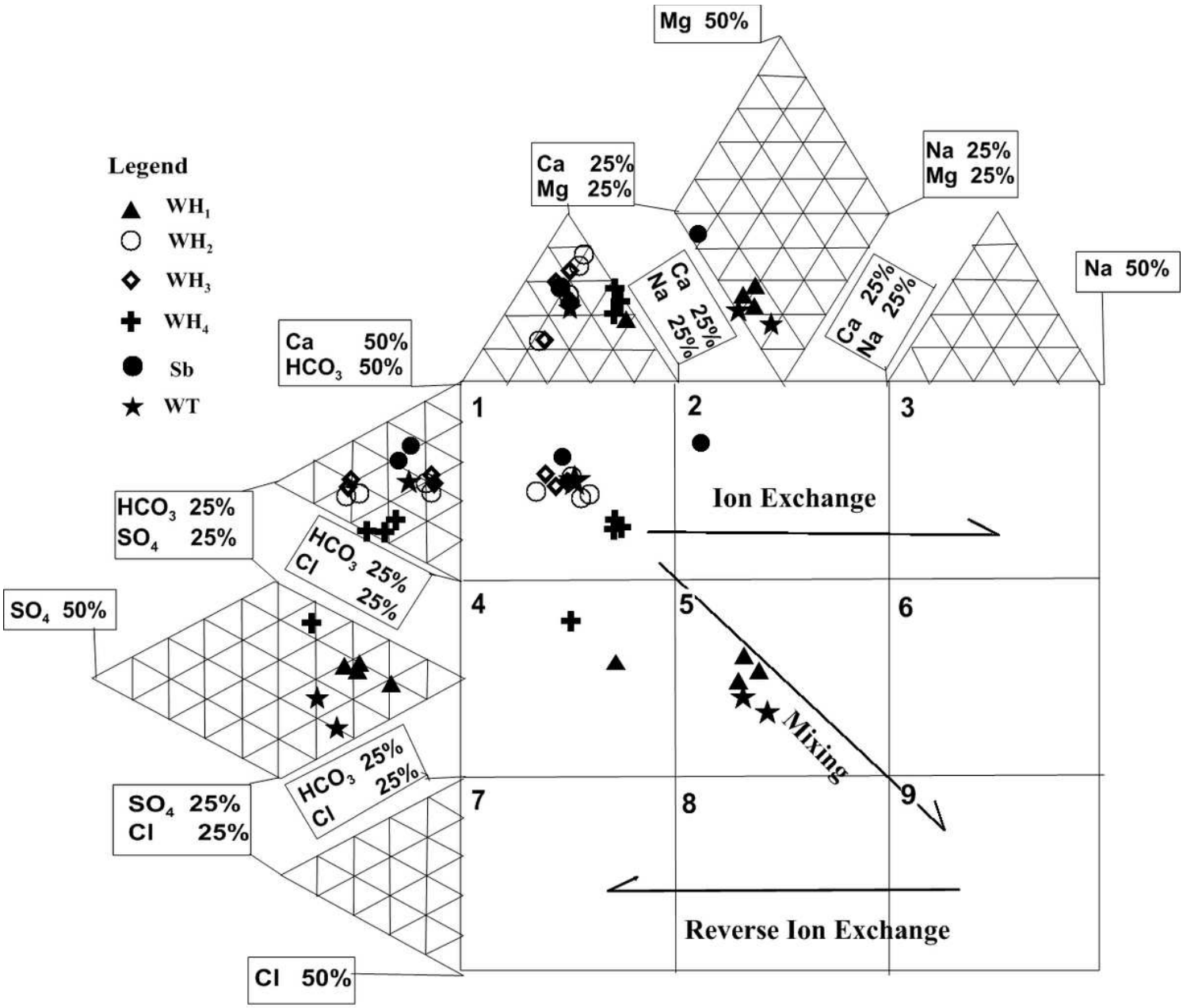

Figure 3

Representation of samples in the expanded Durov diagram

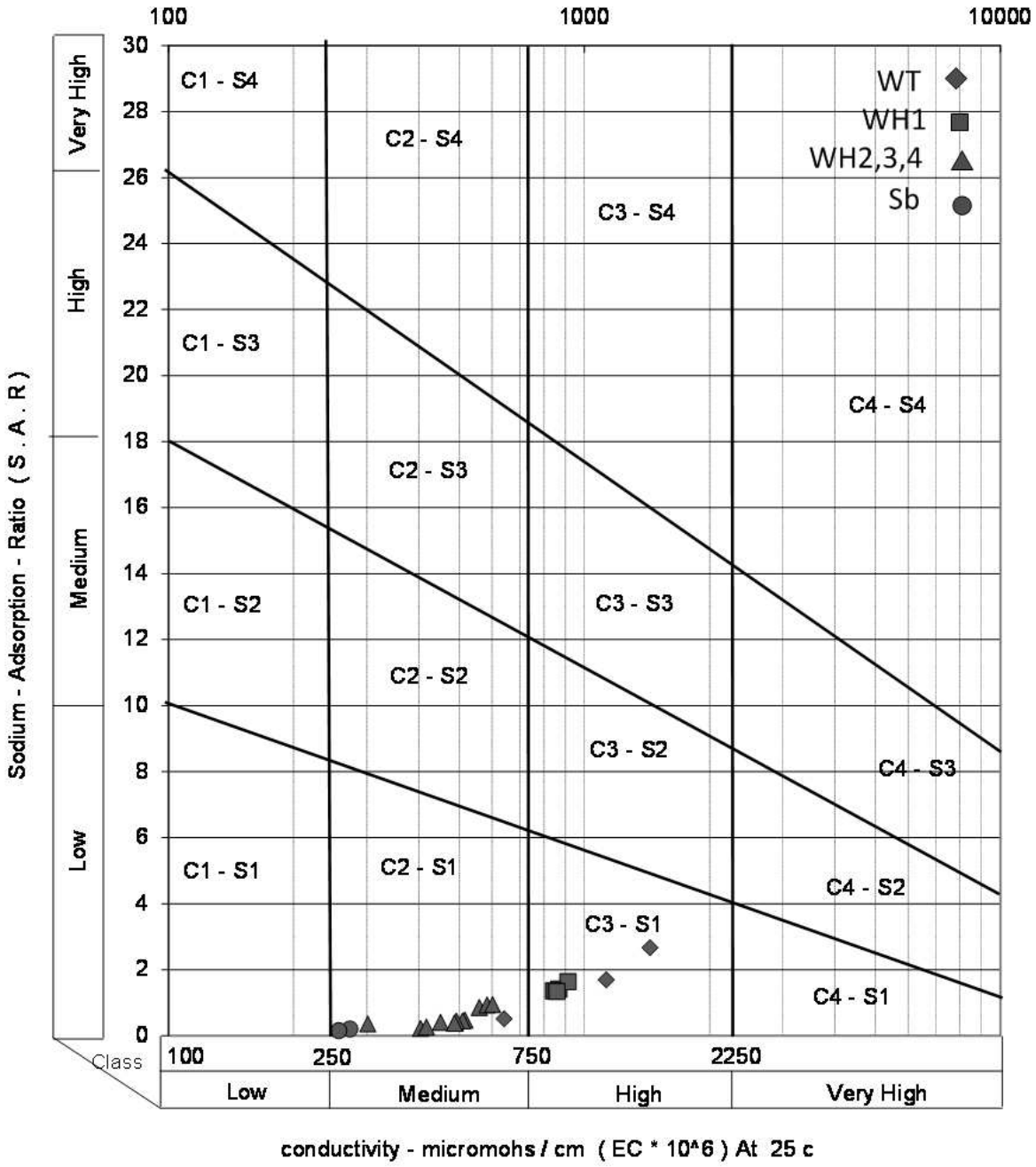

Figure 4

. Diagram of salinity risk and alkalinity of agricultural water

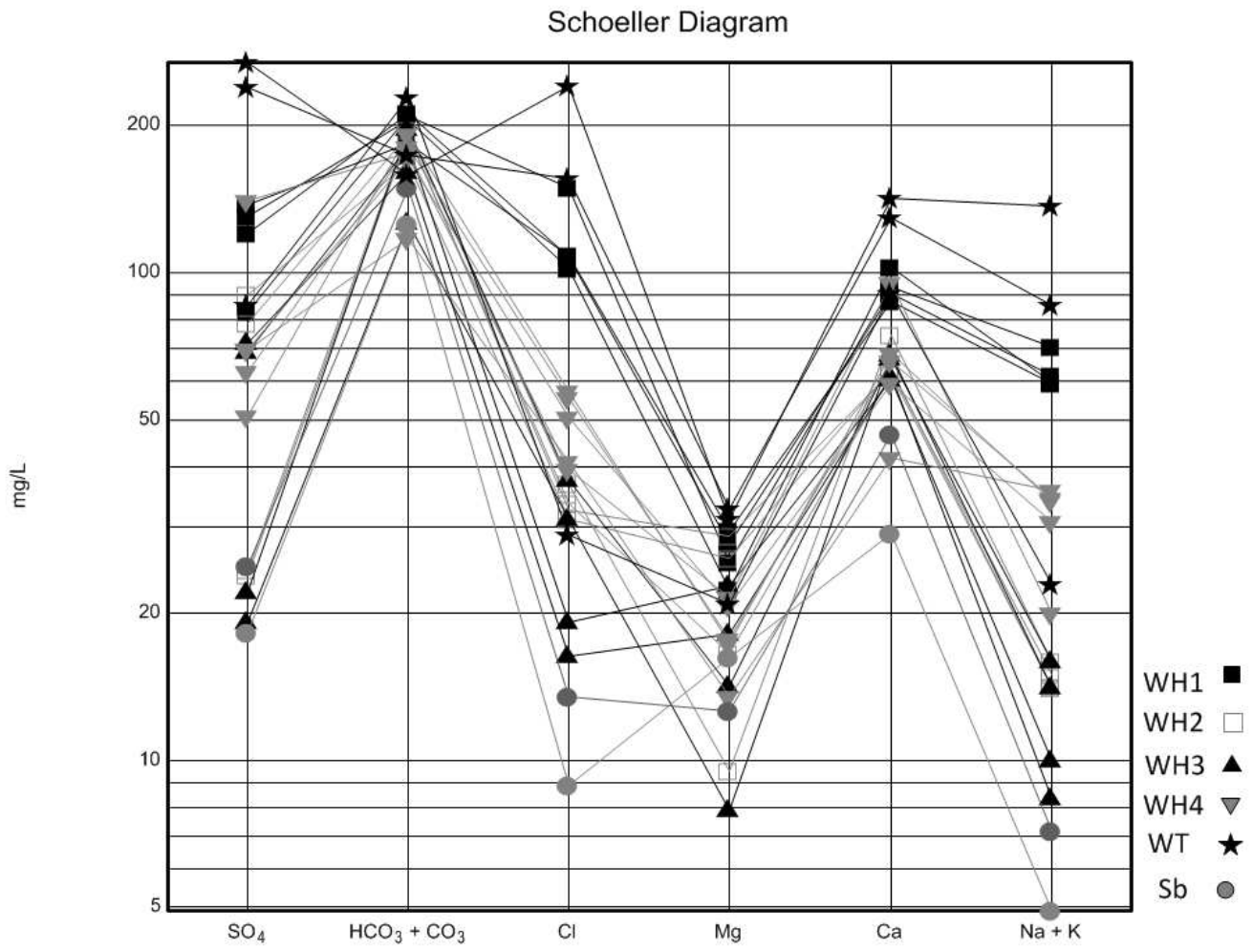

Figure 5

Schuler diagram for water samples in the study area

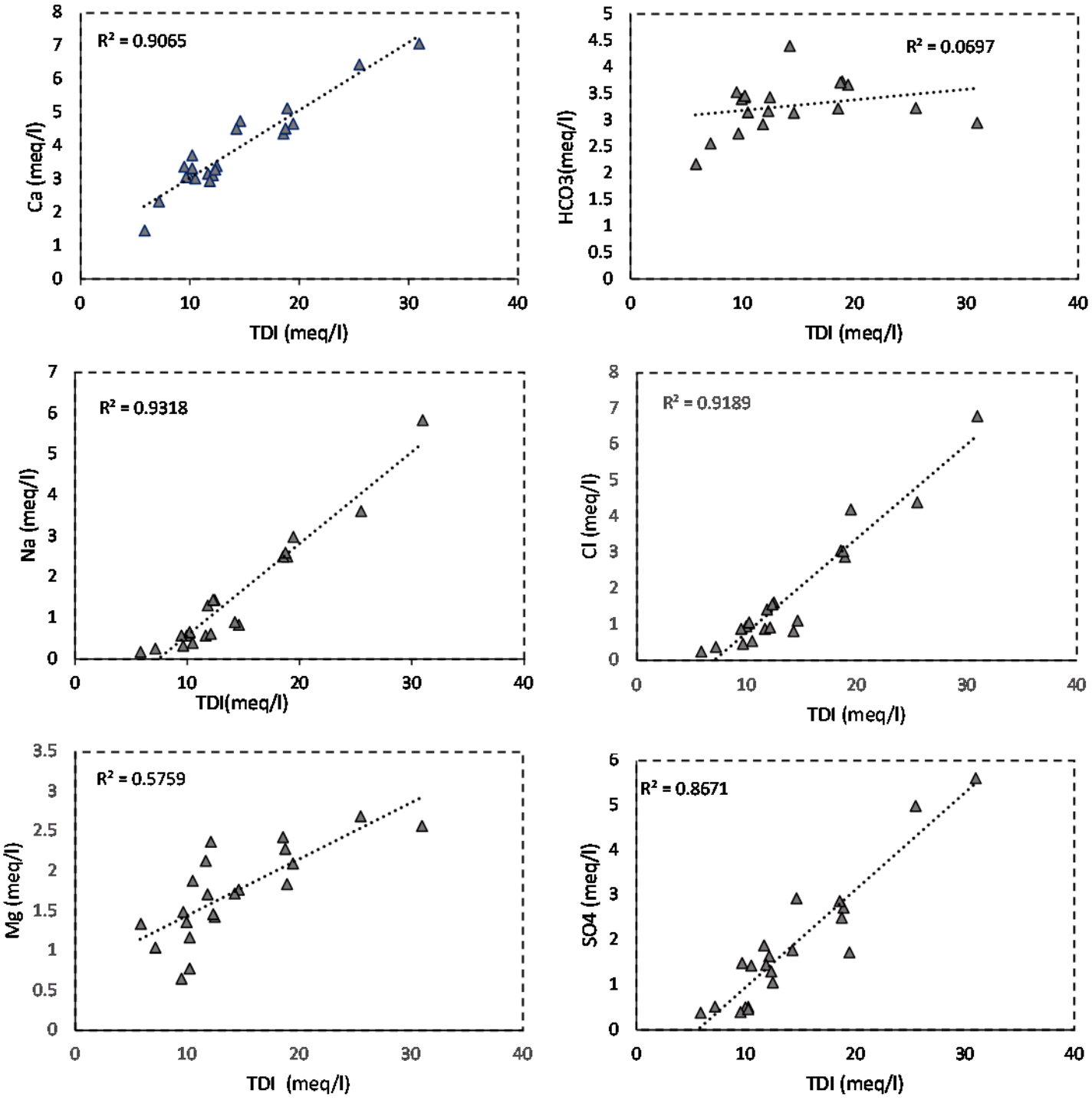

Figure 6

Composite diagrams of the major ions in the samples versus TDI

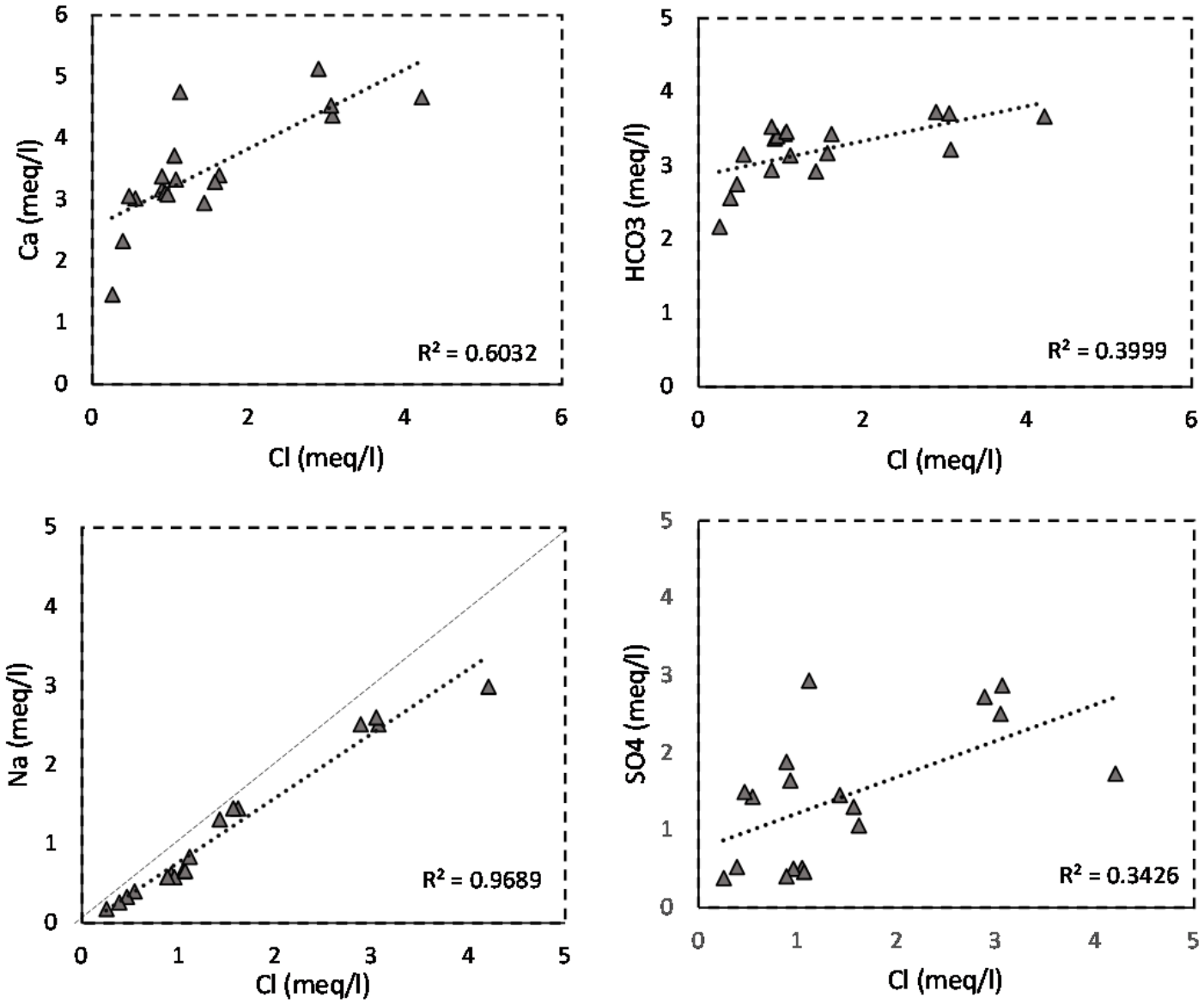

Figure 7

Composite diagram of the major ions versus the chlorine ions

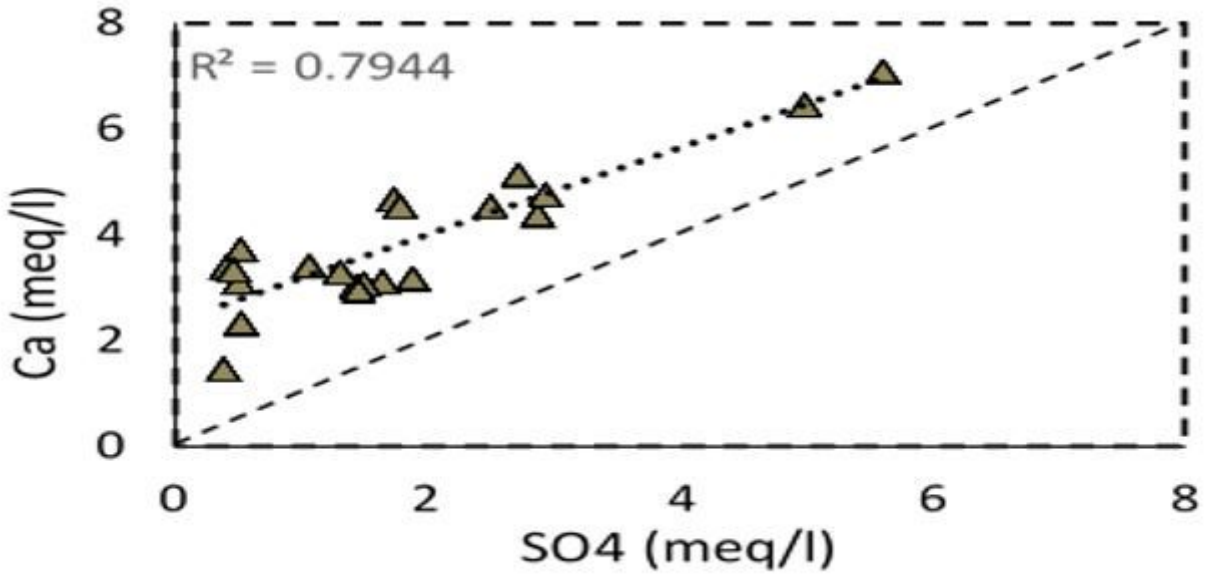

Figure 8

Composite diagram of Ca2 + versus SO42-

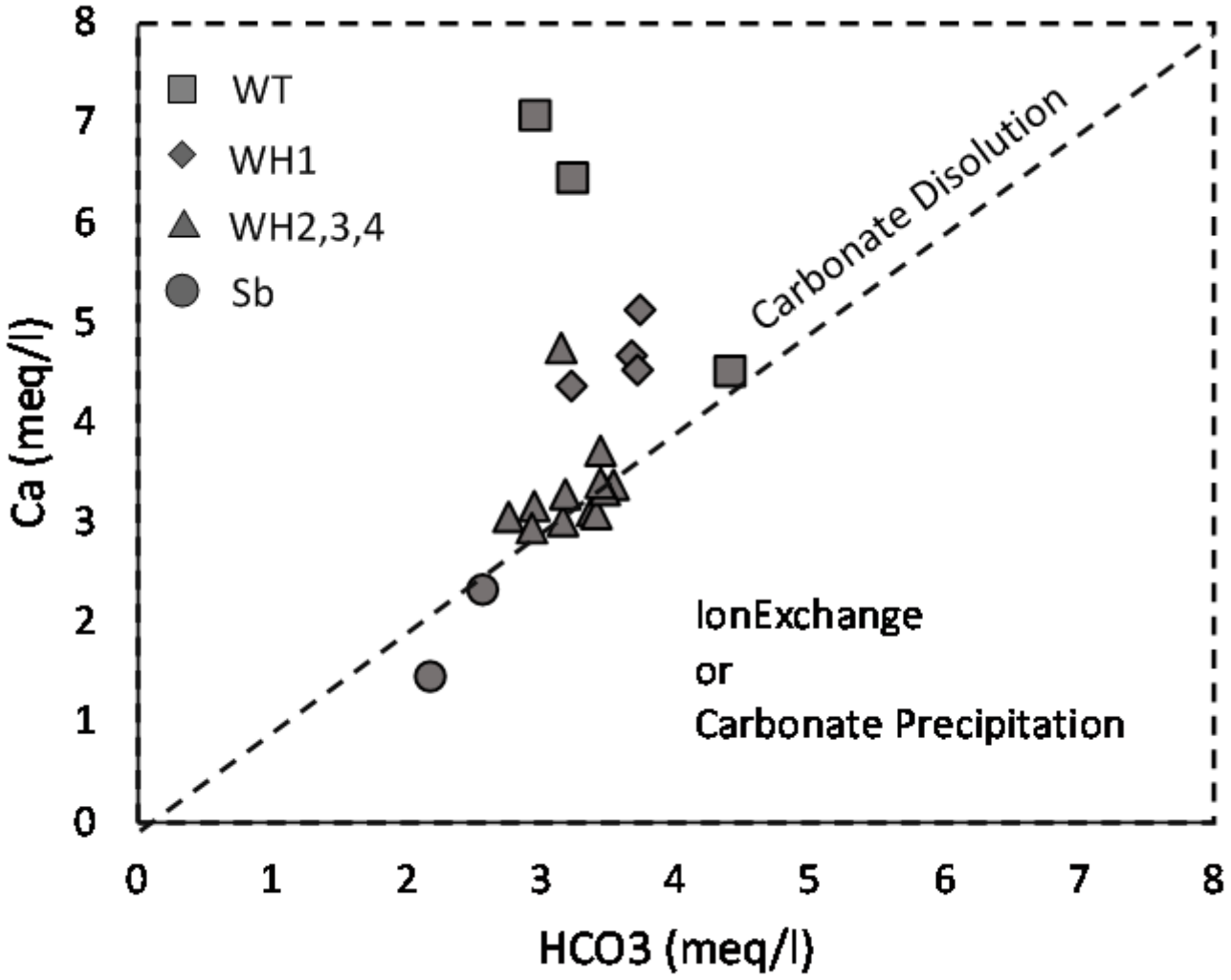

Figure 9

Ion exchange diagrams. Diagram of Ca2 + vs. HCO32

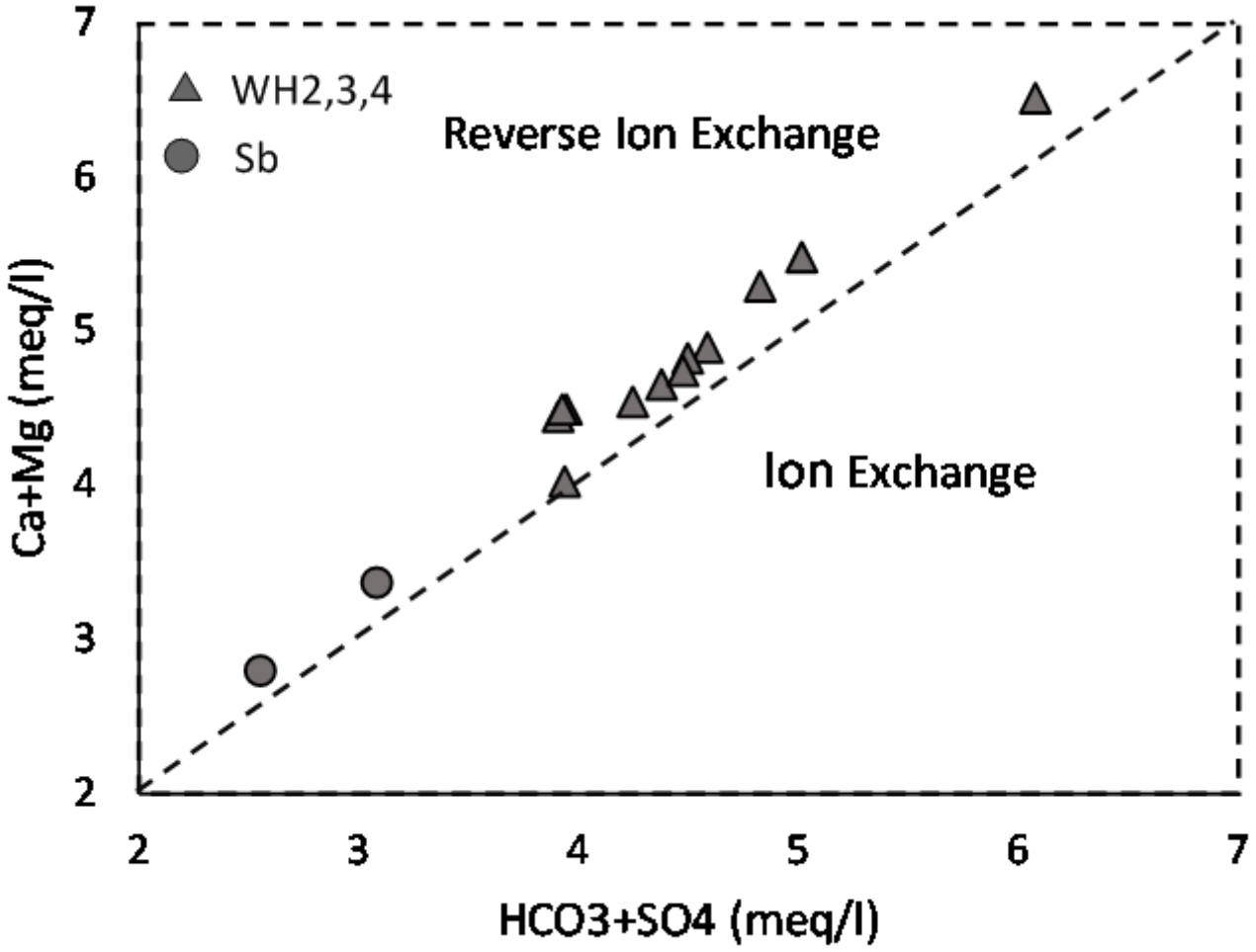

Figure 10

Diagram of Ca2 ++ Mg2 + vs. HCO32- + SO42- for WH2, WH3, WH4, Sb

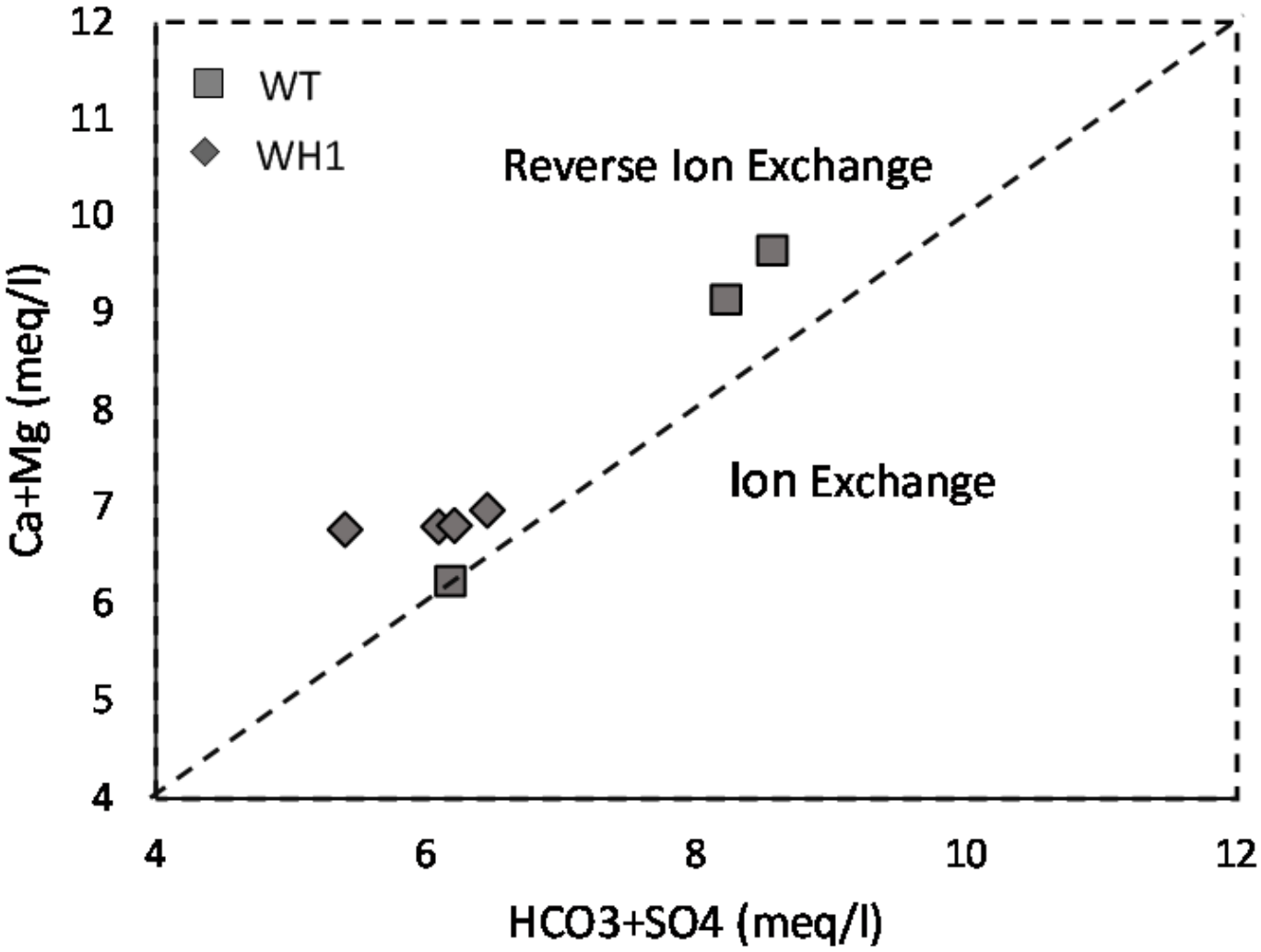

Figure 11

Diagram of Ca2 ++ Mg2 + vs. HCO32- + SO42- for WH1, WT

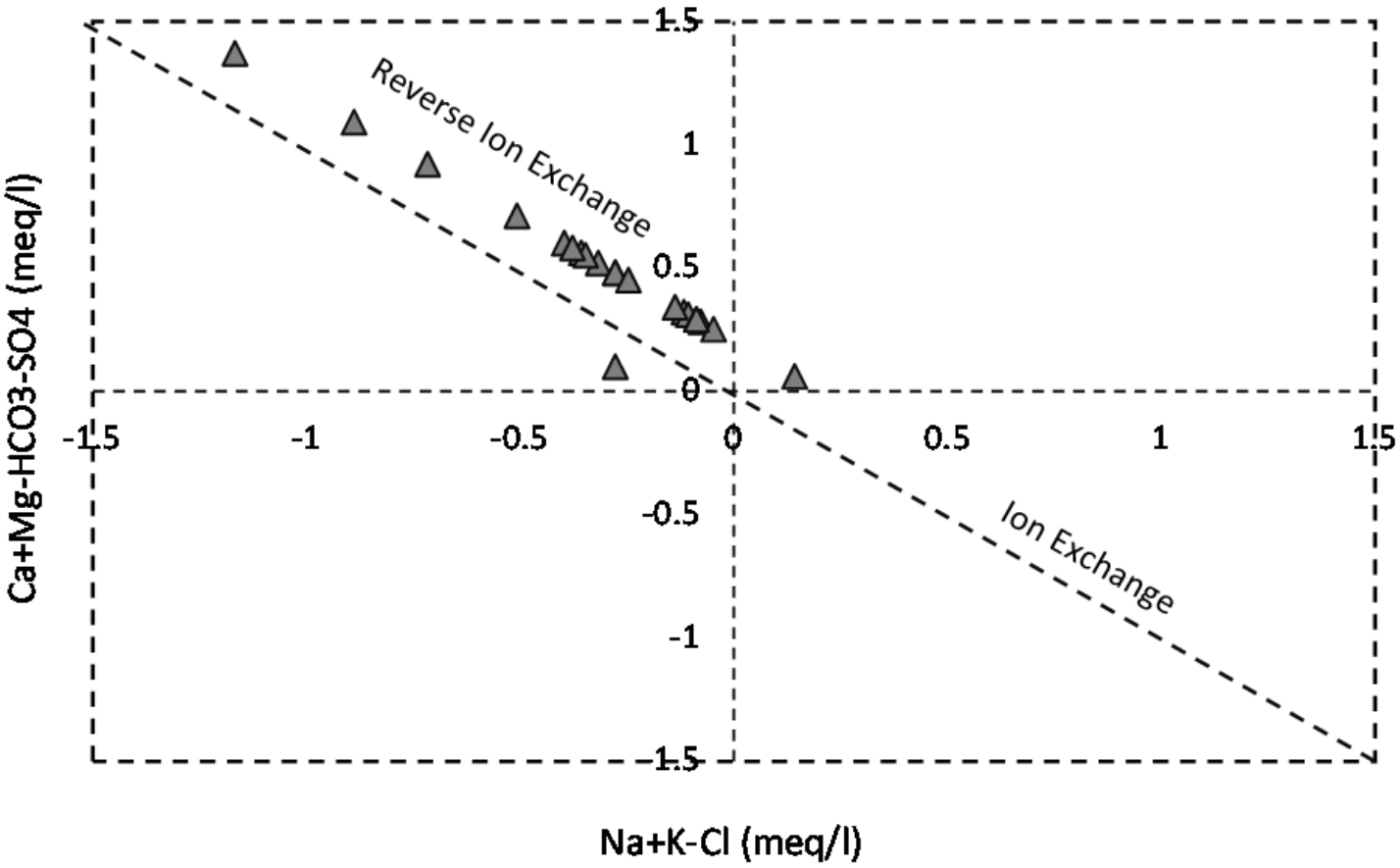

Figure 12

Diagram of Na ++ k + -Cl- vs. HCO32-+SO42- -Ca2+-Mg2+

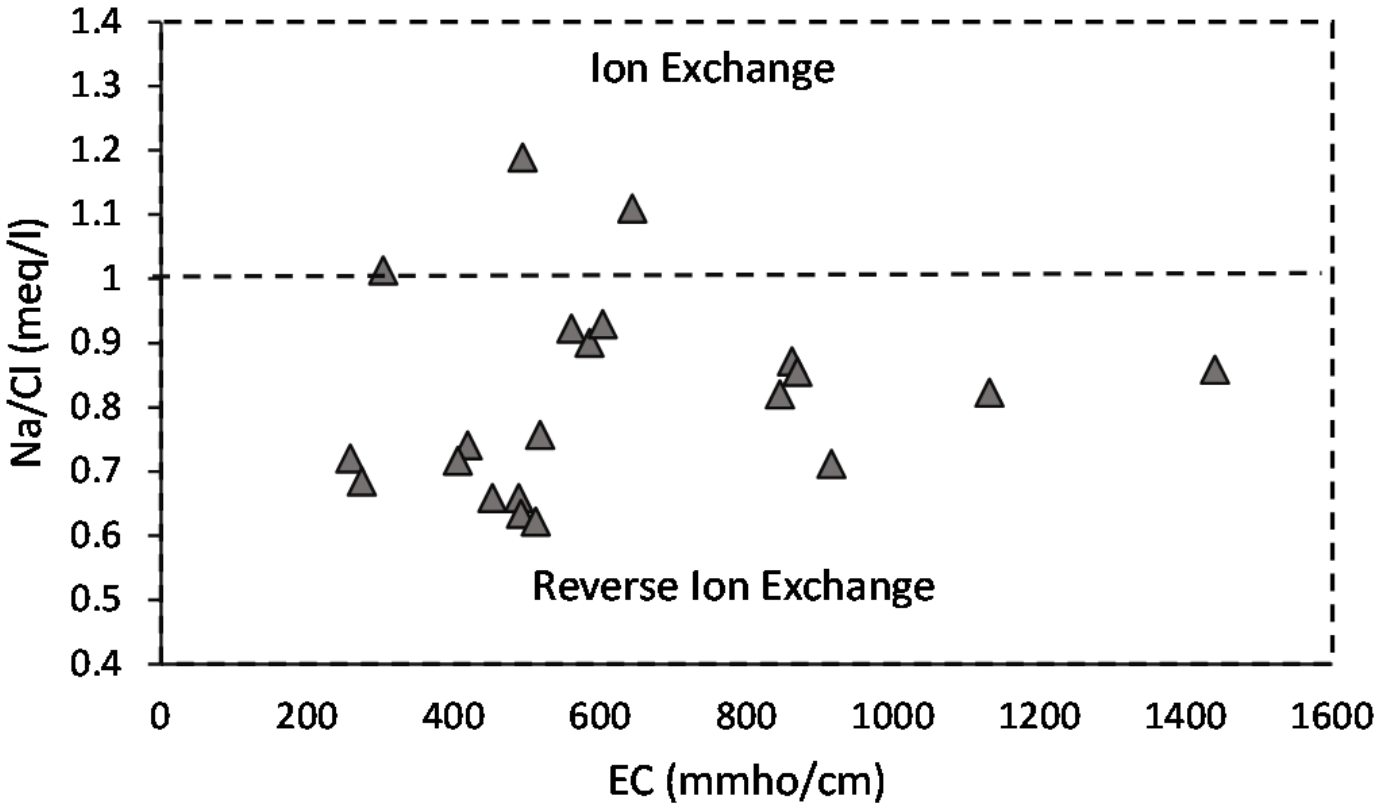

Figure 13

Na/Cl diagram vs. EC

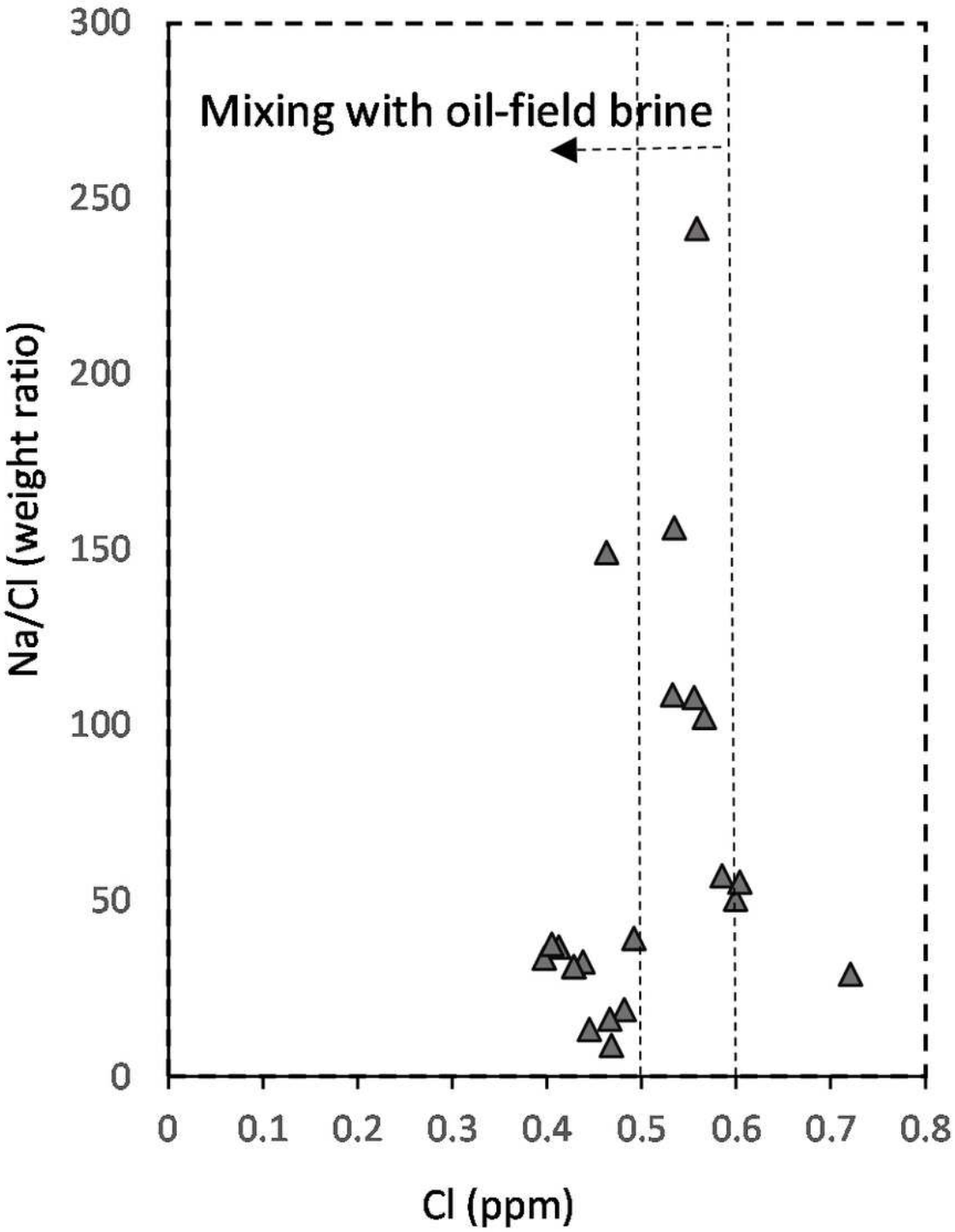

Figure 14

The graph of the Na/Cl ratio versus Cl- in terms of weight ratio

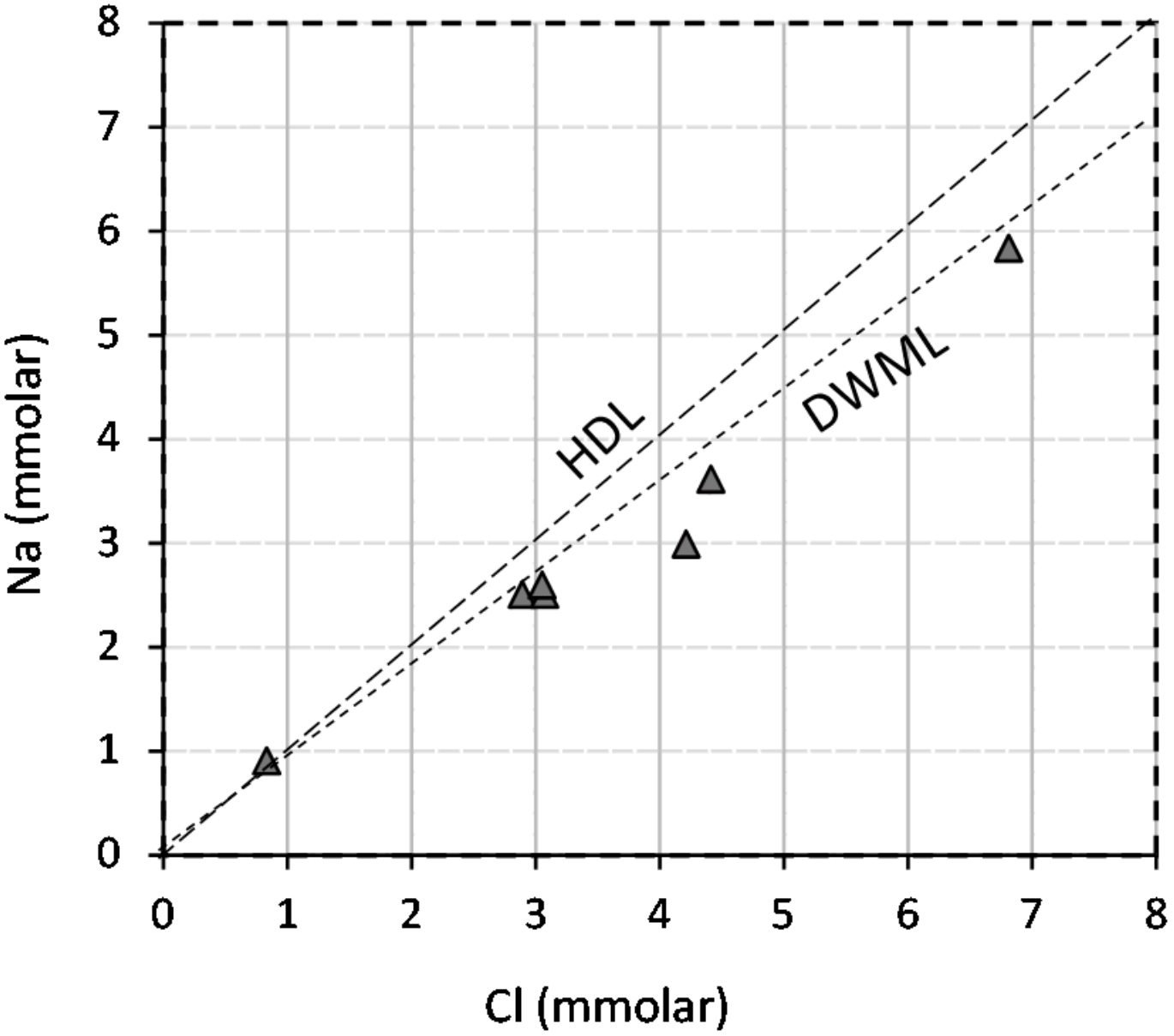

Figure 15

Diagram of Na+ ratio to Cl- of WT and WH1 samples

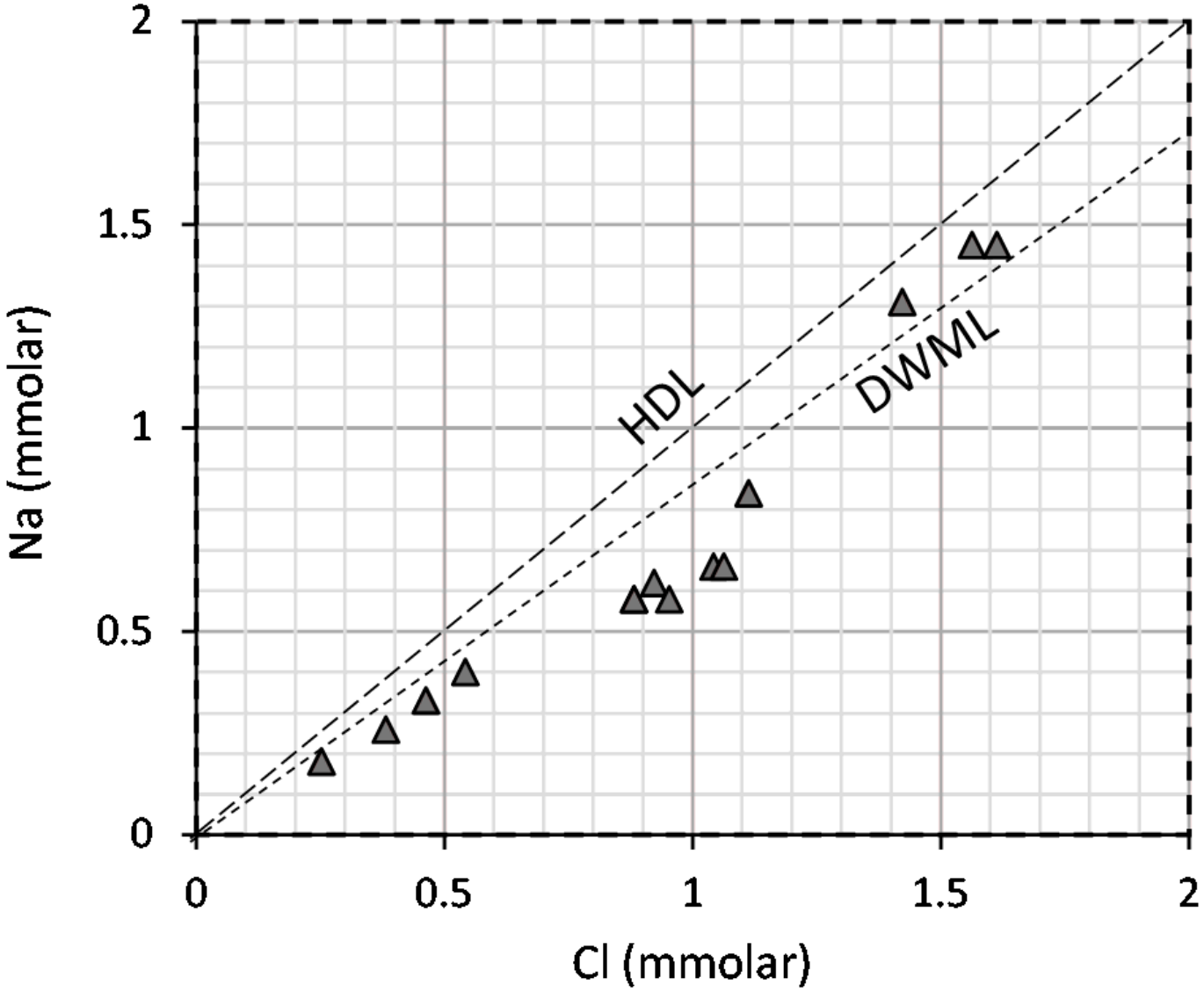

Figure 16

The graph of the Na + ratio to Cl- of samples in WH2, WH3, WH4, Sb

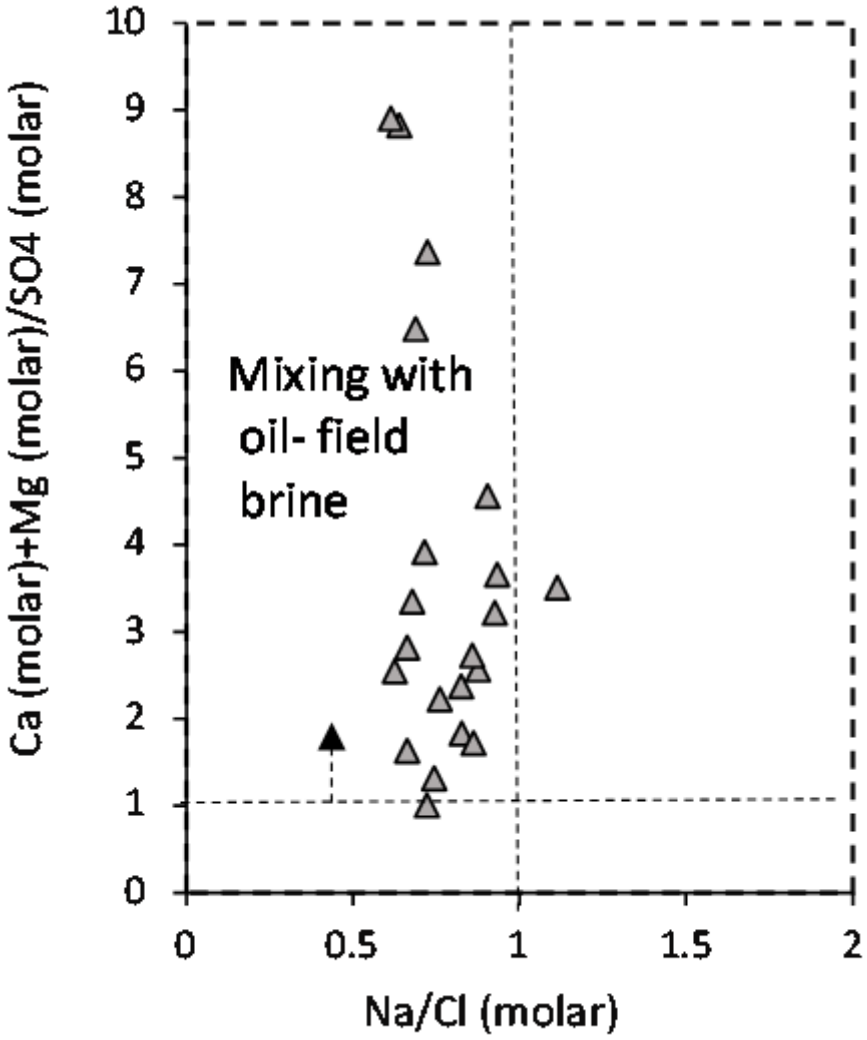

Figure 17

(Ca + Mg) / SO4 diagram vs. Na/Cl

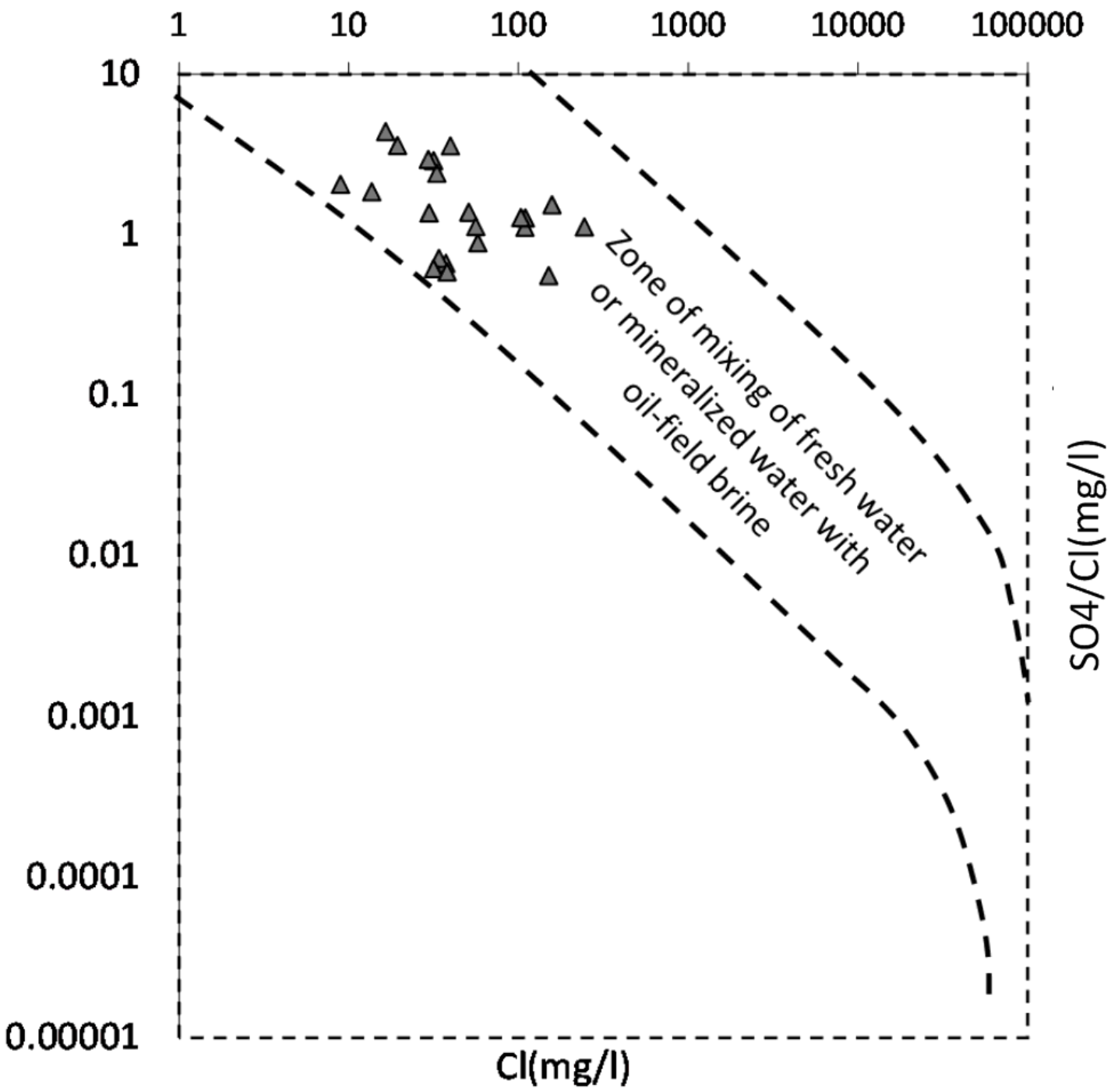

Figure 18

Diagram of the ion ratio of SO4/ Cl to Cl- in terms of weight ratio

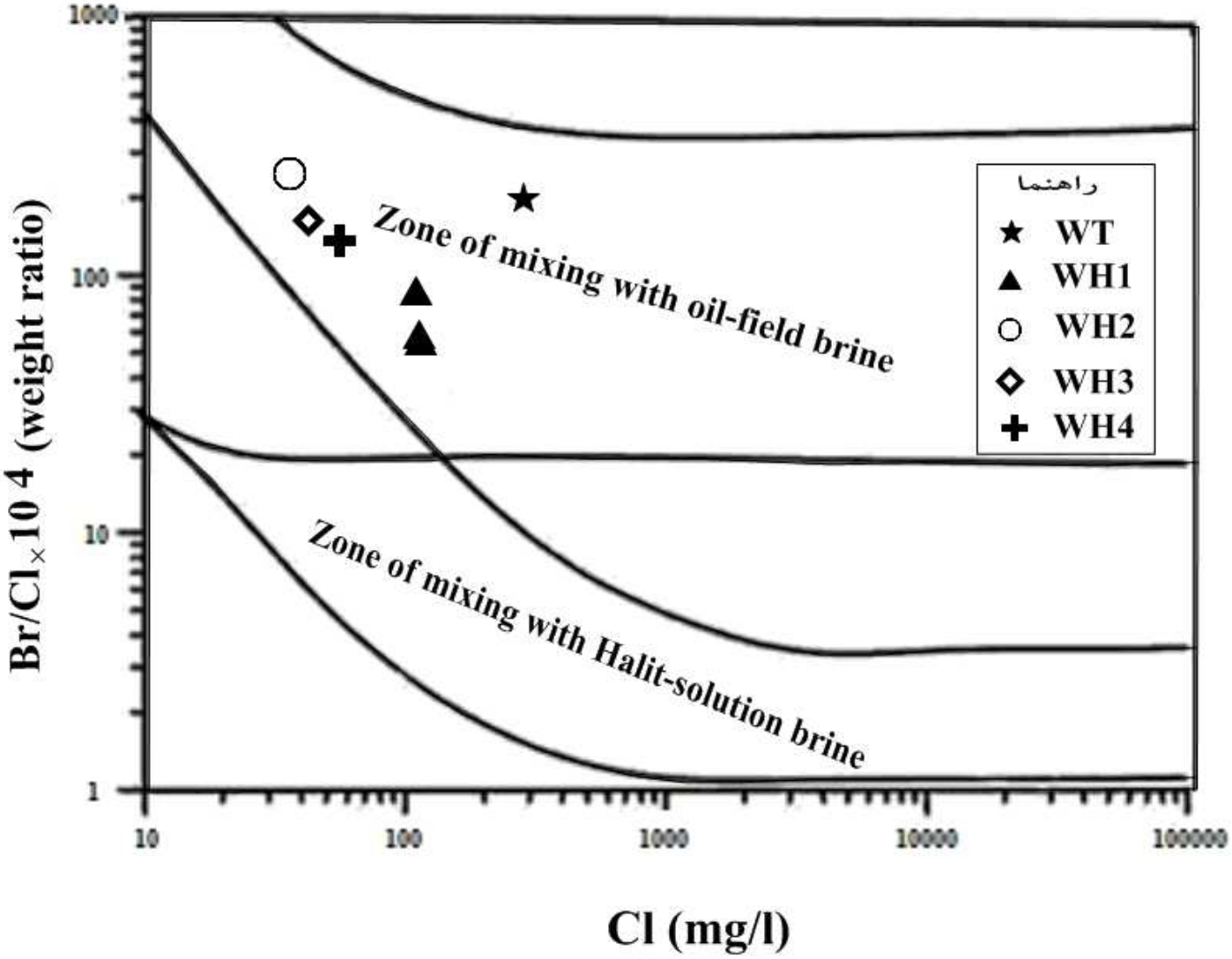

Figure 19

Br/Cl ratio diagram versus Cl in weight ratio